nature genetics

Article

https://doi.org/10.1038/s41588-023-01626-1

Integrative functional genomic analyses identify genetic variants influencing skin pigmentation in Africans

Received: 15 September 2022

Accepted: 28 November 2023

Published online: 10 January 2024

Check for updates

Yuanqing Feng[1], Ning Xie[1], Fumitaka Inoue[2,3,14], Shaohua Fan[1,15], Joshua Saskin[4], Chao Zhang[1], Fang Zhang[1], Matthew E. B. Hansen[1], Thomas Nyambo[5], Sununguko Wata Mpoloka[6], Gaonyadiwe George Mokone[7], Charles Fokunang[8], Gurja Belay[9], Alfred K. Njamnshi[10], Michael S. Marks[11], Elena Oancea[4], Nadav Ahituv[2,3] & Sarah A. Tishkoff[1,12,13]

Skin color is highly variable in Africans, yet little is known about the underlying molecular mechanism. Here we applied massively parallel reporter assays to screen 1,157 candidate variants influencing skin pigmentation in Africans and identified 165 single-nucleotide polymorphisms showing differential regulatory activities between alleles. We combine Hi-C, genome editing and melanin assays to identify regulatory elements for *MFSD12*, *HMG20B*, *OCA2*, *MITF*, *LEF1*, *TRPS1*, *BLOC1S6* and *CYB561A3* that impact melanin levels in vitro and modulate human skin color. We found that independent mutations in an *OCA2* enhancer contribute to the evolution of human skin color diversity and detect signals of local adaptation at enhancers of *MITF*, *LEF1* and *TRPS1,* which may contribute to the light skin color of Khoesan-speaking populations from Southern Africa. Additionally, we identified *CYB561A3* as a novel pigmentation regulator that impacts genes involved in oxidative phosphorylation and melanogenesis. These results provide insights into the mechanisms underlying human skin color diversity and adaptive evolution.

Human skin color displays remarkable diversity across different populations and is hypothesized to be an adaptation to solar ultraviolet radiation[1,2]. Recent genome-wide association studies (GWAS) have shed light on the genetic basis of human skin color variation[3–12]. However, there have been relatively few GWAS in ethnically diverse Africans[5,13] despite the high levels of variation in skin pigmentation in Africa. Indeed, the genetic basis and evolutionary history of skin color in the Khoesan-speaking populations (San) from Southern Africa, who have the oldest genetic lineages and the most lightly pigmented skin observed in Africa[5,13], remain an enigma. Additionally, only a few of the candidate variants associated with human skin pigmentation have been thoroughly investigated through functional experiments[14–17]. Furthermore, previous functional studies mainly focused on variants identified in Europeans, and the molecular mechanisms underlying skin color variation in diverse Africans are still poorly defined[5,13].

In this article, we utilize functional genomics to identify new regulatory variants and genes that influence skin pigmentation in geographically and ethnically diverse Africans. We first selected 29,419 candidate variants, composed of 9,913 variants identified from GWAS of African skin color[13] and 19,553 genetic variants showing extreme allele frequency differences between the lightly pigmented San and other darkly pigmented African populations[18]. We then applied massively parallel reporter assays (MPRA)[19] to measure the regulatory activities of 1,157 single-nucleotide polymorphisms (SNPs) residing in open chromatin regions of melanocyte-derived cells and identified 165 variants with significant differential regulatory effects.

A full list of affiliations appears at the end of the paper. e-mail: tishkoff@pennmedicine.upenn.edu

Using chromosome conformation capture assays and clustered regularly interspaced short palindromic repeats (CRISPR)-based experiments, we characterized the enhancers and variants regulating the expression of genes related to pigmentation and demonstrated their impact on melanin levels in vitro. Overall, these findings offer valuable insights into the genetic basis of skin pigmentation in African populations.

Results

Identification of candidate regulatory variants impacting skin color

To identify SNPs associated with skin pigmentation in Africa, we first performed GWAS of skin color using an imputed dataset in 1,544 eastern and southern African individuals originating from Ethiopia, Tanzania and Botswana[13] (GWAS-All, Supplementary Fig. 1, Supplementary Table 1 and Supplementary Note 1) or a subset of 500 individuals from Botswana (GWAS-Bots, Supplementary Fig. 2 and Supplementary Table 2). We further identified SNPs with significant allele frequency differences in the lightly pigmented southern African San compared with other darkly pigmented African populations based on the Di statistic[18,20] (Di-SNPs, Supplementary Fig. 3 and Supplementary Note 2), which may be enriched for SNPs that are targets of local adaptation and impact the light skin color of the San. To identify variants that may impact enhancer activity, we overlapped the top GWAS-SNPs and Di-SNPs with open chromatin regions from melanocyte-derived cell lines (Fig. 1a and Methods). After filtering, we obtained a total of 1157 SNPs for MPRA, including 340 GWAS-All SNPs, 289 GWAS-Bots SNPs and 536 Di-SNPs (Fig. 1a).

We applied MPRA to screen for enhancer elements and identify SNPs with variants that show significant differential regulatory activity (Methodsand Supplementary Notes 3and 4). Specifically, we constructed a MPRA library using synthesized 200-bp oligos centered on each of the two alleles of the 1157 candidate SNPs, along with 150 negative control and 32 positive control oligos (Supplementary Table 3 and Extended Data Fig. 1). We used this library to perform MPRA in two melanoma cell lines: darkly pigmented MNT-1 cells and lightly pigmented WM88 cells (Fig. 1b and Supplementary Figs. 4 and 5). To identify regulatory regions in MNT-1, we conducted CUT&RUN assays using antibodies against H3K4me3, H3K27ac, MITF and SOX10 (Supplementary Fig. 6). We further performed assays for transposase-accessible chromatin with sequencing (ATAC-seq) in both MNT-1 and WM88, and identified 99,718 and 118,486 open chromatin regions, respectively. We found that only 35% of ATAC-seq peaks are shared between these two cell lines (Supplementary Fig. 6b). To decipher the target genes of the candidate SNPs, we constructed a high-resolution chromatin interaction map of MNT-1 cells using Hi-C and Hi-C combined with H3K27ac chromatin immunoprecipitation (HiChIP) (Methods, Supplementary Note 5 and Supplementary Figs. 7–9).

We used 'mpralm'[21] to identify MPRA functional variants (MFVs), which show significant differential regulatory activity between alternative and reference alleles ('allelic skew'). Out of the 1157 tested SNPs, we identified 106 MFVs in MNT-1 and 104 MFVs in WM88, with 45 MFVs shared in both cell lines, for a total of 165 MFVs (Fig. 1c and Supplementary Table 4). Of the 165 MFVs, 77 are Di-SNPs and 88 are GWAS-SNPs (Fig. 1c), indicating that Di analysis and GWAS are complementary methods for identifying potential functional variants related to skin pigmentation. We observed a moderate correlation between the variant effect sizes in MNT-1 and WM88 ($R = 0.41$, $P = 2.6 \times 10^{-46}$), and 86% of the tested variants showed the same direction of allelic skew (determined by $\log_2$fold change ($\log_2$FC)) in both cell lines (Fig. 1d). Interestingly, rs7948623 (chr11:61137147) near *DDB1* and rs6510760 (chr19:3565253) near *MFSD12* have the largest effect size in MNT-1 and WM88, respectively (Fig. 1e,f), suggesting that these two GWAS-SNPs may be causal variants at these loci[13]. To validate the allelic skews, we performed luciferase reporter assays (LRAs) on 16 MFVs. Among the 16 tested MFVs, 15 MFVs show significant allelic skew in both MPRA and LRA in at least one cell line (MNT-1 or WM88; Supplementary Table 5 and Supplementary Fig. 10). These results indicate that employing two cell lines for the MPRA may enhance the sensitivity for discovering allelic skewed variants that may show differential activity under different *trans*-environments.

MFSD12 and *HMG20B* are the target genes of rs6510760

MFSD12 facilitates organellar cysteine transport and impacts melanin levels in melanocytes[13,22]. MPRA identified six GWAS MFVs (rs6510709, rs734454, rs10416746, rs7246261, rs142317543 and rs6510760) near *MFSD12* that are not in linkage disequilibrium (LD) with each other ($R^2 < 0.2$; Extended Data Fig. 2 and Supplementary Fig. 11). The previously reported SNP rs112332856, in strong LD with rs6510760 ($R^2 = 0.8$), showed no effect on the enhancer activity. Notably, rs6510760 had the largest allelic skew in WM88 ($\log_2$FC = 0.6, $P = 3.4 \times 10^{-32}$) and the sixth most significant allelic skew in MNT-1 ($\log_2$FC 0.51, $P = 4 \times 10^{-24}$; Supplementary Table 4). In silico analysis revealed that rs6510760 disrupts the binding motif of aryl hydrocarbon receptor (AHR, Extended Data Fig. 2l), a vital transcription factor involved in melanogenesis[23].

We validated the allelic enhancer activities of four SNPs overlapping regulatory elements upstream of *MFSD12* (rs734454, rs10416746, rs6510760 and rs7246261) using LRA. We found all four SNPs to have significant allelic skew in at least one of the cell lines (Extended Data Fig. 2 and Supplementary Table 5), and all of them are expression quantitative trait loci of MFSD12 based on GTEx data (Supplementary Fig. 12). SNPs rs6510760 and rs7246261 in enhancer 4 (E4) are 104 bp apart but not in LD. We explored their combinatorial effects (GC, AC, GT and AT) using LRA. The derived haplotype AT, associated with dark skin color, exhibits reduced enhancer activity compared with the GC haplotype (Supplementary Fig. 13). The results suggest that rs6510760 is the major regulator of enhancer activity, while rs7246261 only has marginal additive effects.

We further applied Hi-C and CRISPR experiments to identify the target genes of rs6510760. Hi-C showed interactions between E4 and the promoters of *MFSD12* and *HMG20B* genes (Extended Data Fig. 3a,b and Supplementary Table 6). Compared with controls, CRISPR inhibition (CRISPRi) of E4 significantly reduced the expression of *MFSD12* and *HMG20B* (Extended Data Fig. 3c–e), confirming that E4 interacts with both genes. Downregulation of *MFSD12* expression slightly increased melanin levels in MNT-1 (Extended Data Fig. 3f), consistent with previous reports[13,22]. CRISPR knockout (CRISPR-KO) of E4 in MNT-1 significantly reduced the expression of *MFSD12* and *HMG20B* (Extended Data Fig. 3g). Together, we validated that rs6510760 is the major regulatory variant affecting the activity of E4, which impacts the expression of the *MFSD12* and *HMG20B* genes and contributes to African skin color variation.

Identification of enhancers and regulatory variants near *OCA2*

OCA2 is the causal gene for oculocutaneous albinism II, which affects human skin, hair and eye color[8,13,24–26]. We examined the regulatory activities of ten Di-SNPs and 16 GWAS-SNPs near *OCA2* using MPRA and identified 4 MFVs (rs4778242 in E1, rs6497271 in E2, rs7495989 in E3 and rs4778141 in E4; Fig. 2a and Extended Data Fig. 4). These four MFVs showed strong associations with African skin color ($P < 3.4 \times 10^{-5}$, Fig. 2b and Supplementary Fig. 14) but were not in LD ($R^2 < 0.2$, Supplementary Fig. 15) with the previously reported functional SNPs rs12913832 (ref. 16) and rs1800404 (ref. 13). Among these SNPs, rs6497271 showed the greatest allelic skew in both MNT-1 ($P = 8.9 \times 10^{-17}$, Fig. 2c) and WM88 ($P = 3.2 \times 10^{-4}$).

Using Hi-C[27] and H3K27ac HiChIP[28], we generated a high-resolution (2 kb) chromatin interaction map at the *OCA2*/*HERC2* locus. We identified a topologically associating domain (TAD) encompassing the *OCA2* promoter and its upstream enhancer regions (Fig. 2d and Supplementary Fig. 16) and detected significant interactions between the promoter and enhancer E2 of *OCA2* by FitHiChIP[29] (false discovery rate

https://doi.org/10.1038/s41588-023-01626-1

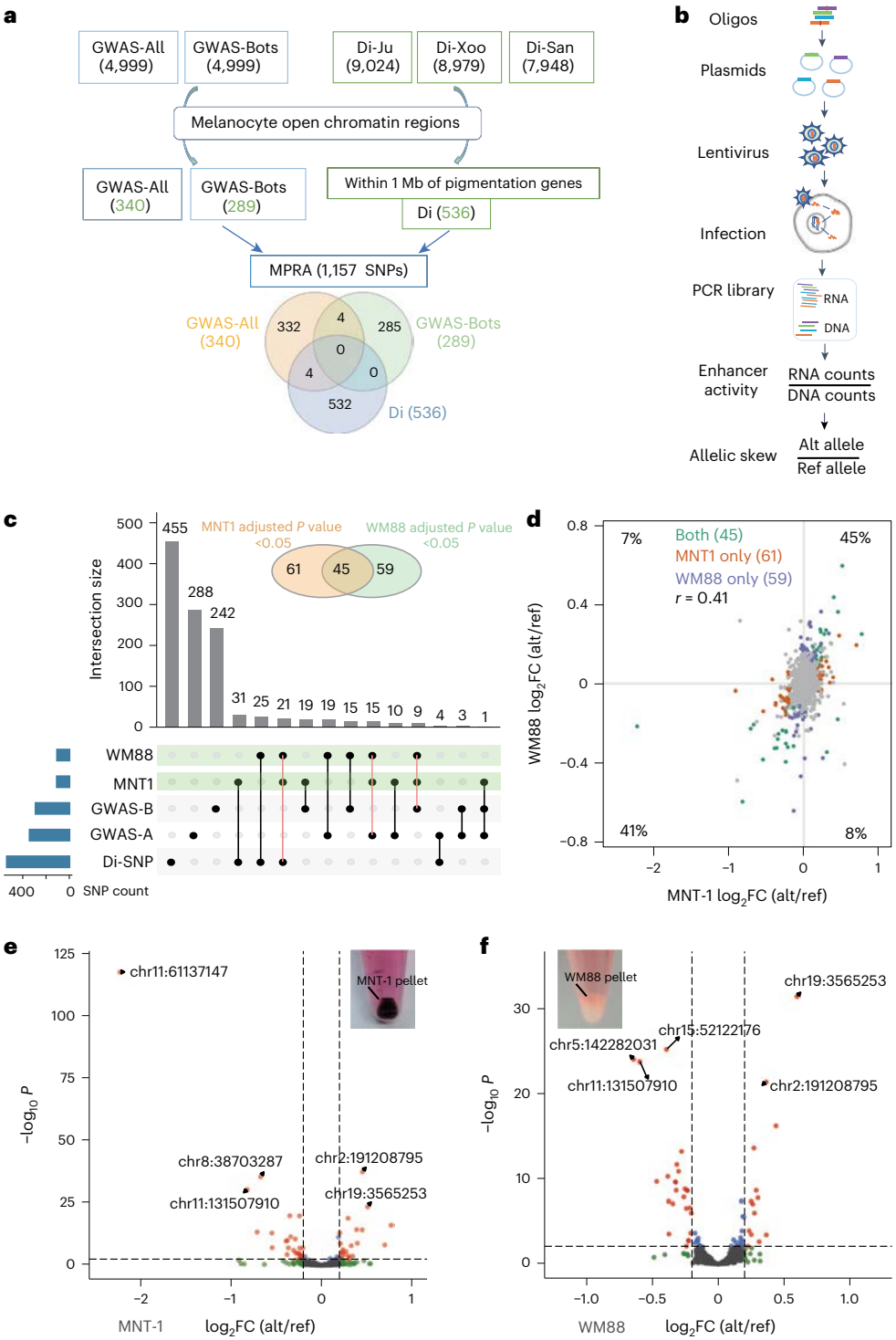

Fig. 1 | Massively parallel screening of genetic variants associated with African skin pigmentation. a, Selection of candidate regulatory variants. GWAS-All are the top 4999 SNPs from GWAS of skin pigmentation in Africans ($P < 2.3 \times 10^{-4}$) and GWAS-Bots are the top 4,999 SNPs from GWAS of skin pigmentation in Botswana ($P < 1.7 \times 10^{-4}$, light-blue boxes). Di-Ju are the top 0.1% Di-SNPs from the Ju|'hoansi versus other populations without inclusion of the !Xoo, Di-Xoo are the top 0.1% Di-SNPs from the !Xoo versus other populations without inclusion of the Ju|'hoansi and Di-San are the top 0.1% Di-SNPs from the Ju|'hoansi and the !Xoo versus other populations (light-green boxes). **b**, Schematic of lentiMPRA workflow. **c**, Upset plot showing the intersections of significant allelic skewed variants from GWAS and Di analysis in MNT-1 and WM88. The alleles with significant differential regulatory activities (adjusted *P* value <0.05) in both MNT-1 and WM88 are highlighted with orange solid lines. GWAS-A represents GWAS-All and GWAS-B represents GWAS-Bots. **d**, Comparison of allelic skews in two melanoma cell lines (MNT-1 and WM88). The percentages are defined by the number of SNPs in each quadrant/total number of SNPs. The alleles with significant differential regulatory activities (adjusted *P* value <0.05) in both cell lines (green), MNT-1 (orange) and WM88 (blue) are highlighted. The nonsignificant alleles are colored in gray. The correlation of allelic skews in MNT-1 and WM88 is estimated by Pearson's $r = 0.41$ ($P = 2.6 \times 10^{-46}$). **e**,**f**, The volcano plots show allelic skewed variants in MNT-1 (**e**) and WM88 (**f**). Allelic skew is defined as the $\log_2$FC of the enhancer activity between the alternative (alt) and reference (ref) alleles (reference alleles match the genome hg19). The locations of the top five SNPs based on the hg19 reference genome are highlighted. Pictures of the cell pellets of MNT-1 and WM88 show that MNT-1 is darkly pigmented and WM88 is nearly nonpigmented.

<0.05, Supplementary Table 6). CRISPRi of E2 caused a 20% decrease of *OCA2* expression (Fig. 2e), validating the promoter–enhancer interaction. Furthermore, RNA sequencing (RNA-seq) showed that CRISPRi of E2 had a significant effect on *OCA2* expression (log_2FC −2.76) but only a marginal effect on *HERC2* expression (log_2FC −0.40), and it altered the expression of melanogenesis-related genes, such as *DCT*, *PMEL* and *TYRP1* (Fig. 2f and Supplementary Fig. 17). Notably, CRISPRi of E2 decreased the melanin level in MNT-1 (Fig. 2g). CRISPR-KO of E2 in MNT-1 decreased the expression of *OCA2* and melanin levels by more than 50% (Fig. 2h,i and Supplementary Fig. 18). Together, these data highlight the strong effect of E2 on *OCA2* expression.

We further conducted CRISPR/Cas9-mediated genome editing and obtained four clones with SNPs at or next to rs6497271 (Fig. 2j). Notably, all four clones show a significant reduction of *OCA2* expression and melanin levels compared with the control (Fig. 2k,l). In silico analysis showed that rs6497271 disrupts the binding motifs of SOX10 and LEF1 (Extended Data Fig. 4f), which are key transcription factors in melanocytes. In addition, rs6497271 overlaps a SOX10 binding peak in MNT-1 (Fig. 2a). Thus, the substitution from A to G and the indels at rs6497271 may affect the binding of SOX10, reducing the enhancer activity and subsequent *OCA2* expression. In addition, UK Biobank (UKBB) GWAS data[7,30] showed that rs6497271-G is associated with both light skin color and light hair color, indicating that rs6497271 has pleiotropic effects (Supplementary Fig. 19). Collectively, we identified rs6497271 at *OCA2* as a major functional variant affecting human skin pigmentation.

Repeated mutation of an *OCA2* enhancer during human evolution

SNP rs12913832 is a known functional variant associated with blue eye color in Europeans[16] and is 187 bp away from rs6497271. Based on 1000G (ref. 31) and African 5M SNP array (5M) (ref. 13) datasets, the derived allele rs6497271-G is almost fixed (0.984) in Europeans, whereas the ancestral allele rs12913832-A is nearly fixed (0.976) in Africans (Fig. 3a). rs6497271 and rs12913832 form four haplotypes (AA, AG, GA and GG), and we tested the combinatorial effects of these haplotypes using LRA. Haplotype AA showed the highest enhancer activity (75-fold of the control in MNT-1), haplotypes AG and GA reduced the enhancer activity to 50–70% of AA and haplotype GG exhibited the lowest enhancer activity (~25% of AA, Fig. 3b). Consistent with these results, haplotype AA is common in Africans (0.24–0.79) and South Asians (0.16) who have relatively dark skin color. Haplotype GA is common in global populations (>0.21) and has the highest frequency in East Asians (0.98) who have moderately pigmented skin; haplotype GG is at a high frequency only in Europeans (0.64) who have light skin color (Fig. 3c,d). To determine when these haplotypes formed during human history, we extracted the estimated ages of these two variants from a dataset based on genealogical inference[32]. The data revealed that the derived allele G at rs6497271 emerged as early as 1.2 million years ago, while the derived allele G at rs12913832 emerged about 57,000 years ago, coinciding with the migration of modern humans out of Africa (Fig. 3e). These observations suggest that the continuous evolution of the E2 enhancer during human history contributes to current human skin color diversity.

A Di-SNP in *MITF* contributes to light skin color in the San

MITF is a master regulator of melanocyte development and proliferation[33]. A cluster of 44 Di-SNPs was identified in the introns of *MITF*, indicating a signature of local adaptation[18] (Fig. 4a and Supplementary Fig. 20). We identified two MFVs: rs111969762 (in E1) and rs7430957 (in E2). Both MFVs are in melanocyte-specific enhancers and colocalize with MITF and SOX10 chromatin immunoprecipitation followed by sequencing (ChIP–seq) peaks (Fig. 4a and Extended Data Fig. 5a). However, LRA showed that only rs111969762 exhibits regulatory activity but not rs7430957 (Fig. 4b,cand Extended Data Fig. 5d). The discrepancy in enhancer activity for rs7430957 in MPRA and LRA could be due to the difference in enhancer lengths or *trans*-environment between the two methods[34]. The enhancer activity of the derived allele rs111969762-T is about threefold higher than that of rs111969762-C (Fig. 4b,c). In addition, the T-to-C mutation at rs111969762 disrupts the binding motif of FOXP3 (Extended Data Fig. 5e), which is a transcription factor affecting pigmentation[35]. The ancestral allele rs111969762-C is rare (frequency <0.05) in most populations but is common in the San (0.47 in Ju|'hoansi and 0.63 in !Xoo; Supplementary Fig. 21 and Supplementary Table 7).

Hi-C identified nested TADs at the *MITF* locus, and H3K27ac HiChIP detected multiple loops within *MITF* (Fig. 4d and Supplementary Fig. 22). Specifically, we observed a significant interaction (false discovery rate <0.05 by cLoops[36], Supplementary Table 6) between rs111969762 and the TSS of the melanocyte-enriched isoform of *MITF* (Fig. 4d). CRISPRi of E1 significantly reduced the expression of *MITF* and melanin levels in MNT-1 (Fig. 4e,f), further validating that E1 interacts with the *MITF* promoter by chromatin looping. CRISPR-KO of E1 also

Fig. 2 | Regulatory variant rs6497271 impacts *OCA2* expression and contributes to human skin color variations. a, MPRA identified four regulatory variants near *OCA2*. MFVs are highlighted in red. Green tracks indicate ATAC-seq for MNT-1 and WM88 cells; blue tracks indicate ATAC-Seq and ChIP-Seq from normal human melanocytes (NHM); orange tracks indicate CUT&RUN from MNT-1 cells. E1–E4 are four enhancers of *OCA2*. **b**, rs6497271 is associated with African skin pigmentation ($n = 1544$). Each dot represents an individual. The AA, AG and GG genotypes at rs6497271 were colored in green, orange and blue, respectively. *P* value was calculated using EPACTS 'q. emmax' method. **c**, MPRA showed that rs6497271 significantly changed the enhancer activities in MNT-1. Each dot represents a unique barcode linked with an oligo harboring rs6497271. Enhancers with A and G allele at rs6497271 are colored in green and orange, respectively. 1_G and 1_A, 2_G and 2_A, 3_G and 3_A are from three independent replicates. Two-tailed unpaired *t*-tests were used for the three biological replicates. **d**, Chromatin interactions near *OCA2* identified by Hi-C and H3K27ac HiChIP using Hae3 digestion. The purple arches are chromatin loops, the four vertical red lines are MFVs identified by MPRA (MPRA_SNPs), the blue track represents DNase-seq of melanocytes (DNase melanocyte), and the orange shadowed line represents enhancer E2. **e**, qPCR showing that CRISPRi of E2 significantly reduces the expression of *OCA2*. CRISPRi was performed in MNT-1. A two-sided Dunnett's test with adjustments for multiple comparisons were performed for the OCA2_E2_sg1 + sg2 group ($n = 3$) and other groups($n = 6$). **f**, RNA-seq data showing CRISPRi of E2 inhibits *OCA2* gene expression. Red dots are genes with $|log_2FC| > 0.5$ and $P < 0.01$; blue dots are genes with $|log_2FC| < 0.5$ and $P < 0.01$; green dots are genes with $|log_2FC| > 0.5$ and $P > 0.01$; black dots are genes with $|log_2FC| < 0.5$ and $P > 0.01$. The *P* value of *OCA2* ($P = 0$) was set to 1×10^{-50} for the plot. *P* values were calculated using DESeq2. **g**, CRISPRi of E2 significantly reduced melanin levels. The CRISPRi was performed in MNT-1 using two sgRNAs (two-tailed unpaired *t*-tests ($n = 19$)). **h**, qPCR showing that CRISPR-KO of E2 significantly decreases the expression level of *OCA2*. The CRISPR-KO was performed in MNT-1 using two sgRNAs. Two-tailed unpaired *t*-tests ($n = 12$) were used. **i**, CRISPR-KO of E2 significantly reduced melanin levels (two-tailed unpaired *t*-tests ($n = 10$)). **j**, Genotyping of four CRISPR-edited MNT-1 clones at rs6497271. The gray line indicates single guide RNA (sgRNA). The 395 bp amplicons flanking rs6497271 were amplified and sequenced using MiSeq. The top two genotypes in each clone are shown. **k**, Mutations near rs6497271 significantly decreased melanin levels in MNT-1. Four clones were selected and compared with nonedited control cells. A two-sided Dunnett's test with adjustments for multiple comparisons ($n = 4$) was performed. **l**, Mutations near rs6497271 significantly reduced the expression of *OCA2* in MNT-1. A two-sided Dunnett's test with adjustments for multiple comparisons for OCA2-E2_C7 ($n = 6$), OCA2-E2_H2 ($n = 8$) and others ($n = 9$) was performed. The data are presented as mean ± s.e.m. The *P* values are listed above the bars. For the boxplots in panels **b** and **c**, the central vertical lines are the median, with the boxes extending from the 25th to the 75th percentiles. The whiskers further extend by ±1.5 times the interquartile range from the limits of each box. In panels **e**, **g**–**i**, **k**, **l**, different experimental groups were colored using different colors; the central vertical lines indicate the standard error of the mean; the *P* values are listed above the bars.

https://doi.org/10.1038/s41588-023-01626-1

significantly reduced the expression of *MITF* and melanin levels in MNT-1 (Fig. 4g,h and Supplementary Fig. 23a). RNA-seq revealed that the E1 knockout affected the expression of genes in the melanosome and melanogenesis pathways (Fig. 4i,j and Supplementary Fig. 23b,c). For example, we observed downregulation of *DCT*, *MC1R*, *PMEL* and *SLC24A5*, which are involved in melanogenesis and pigmentation, and upregulation of *LEF1* and *PAX3*, which are upstream transcriptional activators of *MITF*[37,38]. Collectively, these results indicate that rs111969762

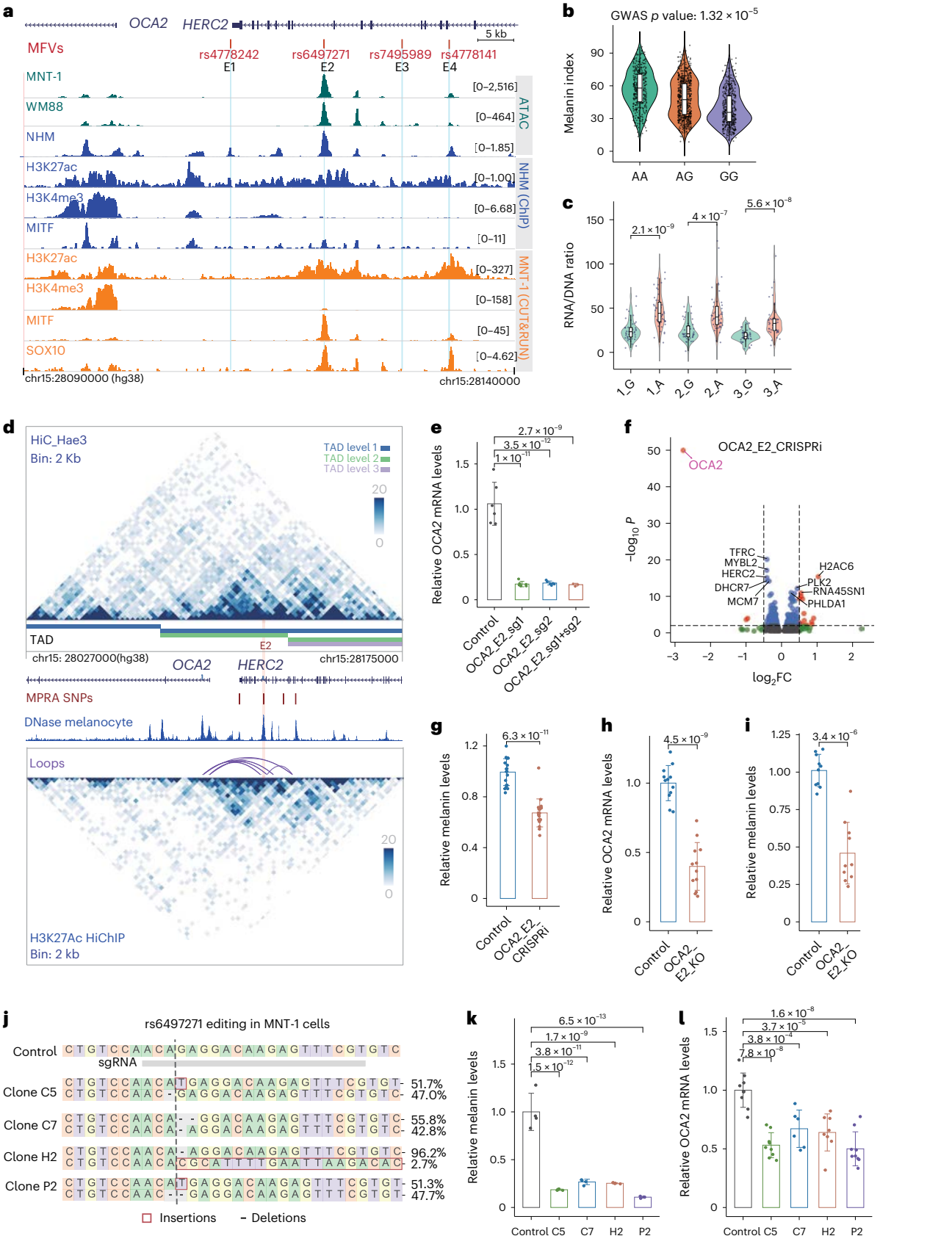

https://doi.org/10.1038/s41588-023-01626-1

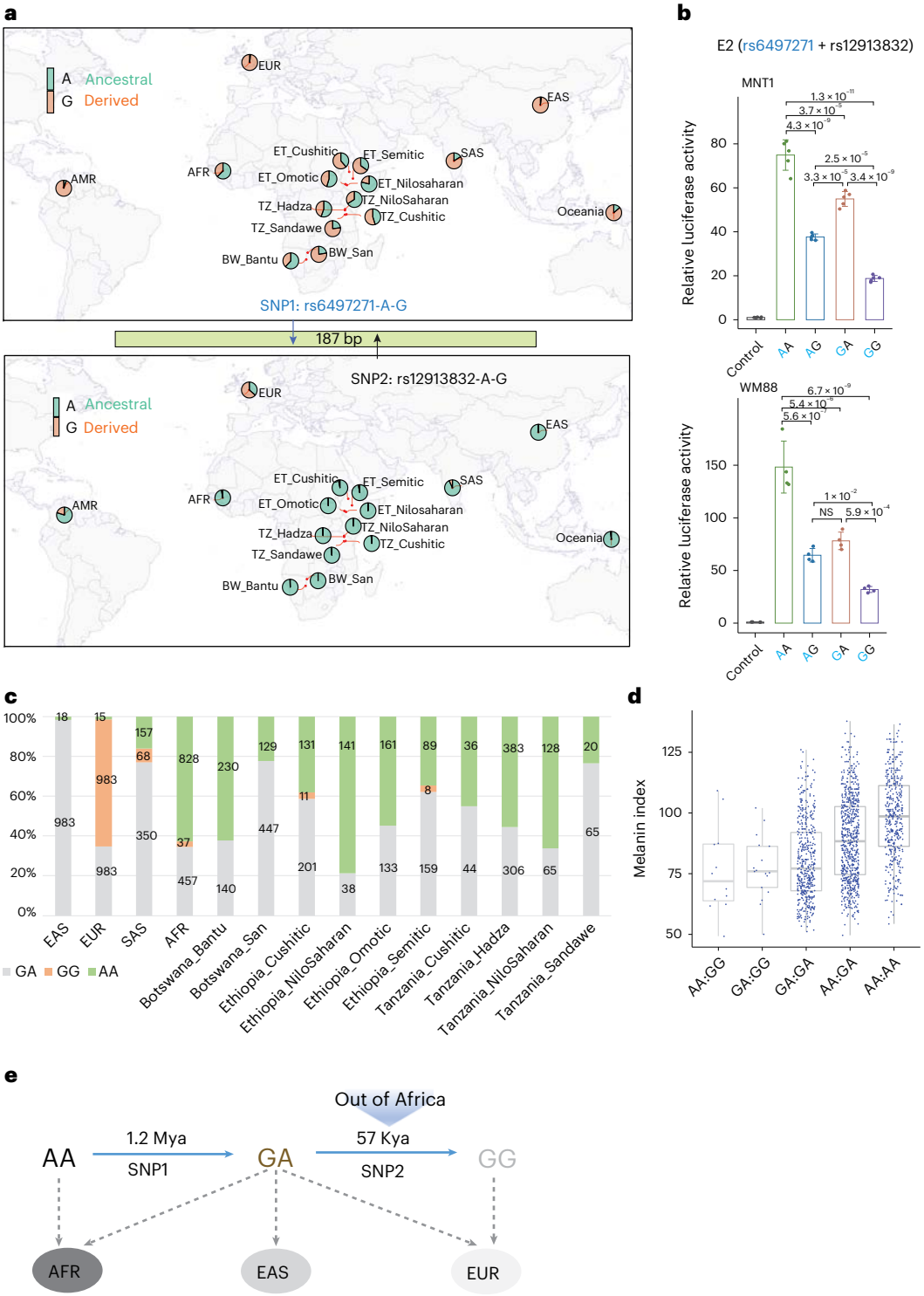

Fig. 3 | Continuing evolution of *OCA2* enhancer E2 contributes to African skin pigmentation diversity. a, Allele frequencies at rs6497271 and rs12913832 in global populations. The derived alleles are colored in orange. The data are merged from 1000G (ref. 31), African 5M (ref. 13) and SGDP[49] datasets. **b**, The enhancer activities of four haplotypes containing rs6497271 and rs12913832 in MNT-1 (top) and WM88 (bottom) estimated by LRA. A two-sided Tukey's test with adjustments for multiple comparisons ($n = 4$) was performed. The data are presented as mean ± s.e.m. (NS, $P > 0.05$). **c**, The frequencies of haplotypes containing rs6497271 and rs12913832 in global populations. The data are merged from 1000G, African 5M and SGDP datasets. **d**, A plot of melanin indexes of individuals with different haplotype combinations at rs6497271 and rs12913832. The data are from GWAS-All ($n = 1,544$). **e**, Estimated ages of SNP rs6497271 and rs12913832 are 1.2 million years ago (Mya) and 57 thousand years ago (Kya), respectively. The data are from https://human.genome.dating/. For the boxplots, the central vertical lines are the median, with the boxes extending from the 25th to the 75th percentiles. The whiskers further extend by ±1.5 times the interquartile range from the limits of each box.

https://doi.org/10.1038/s41588-023-01626-1

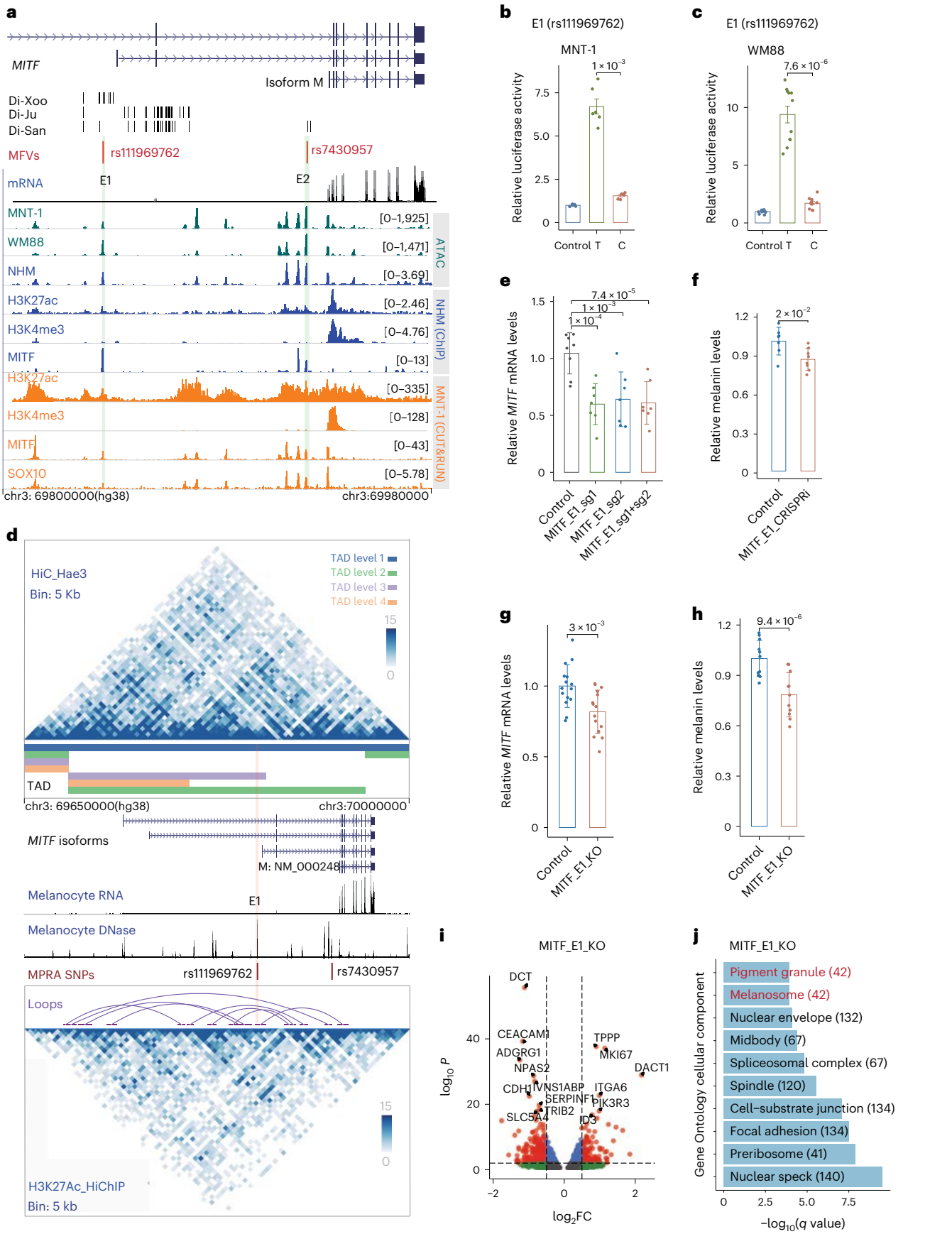

Fig. 4 | Regulatory variant rs111969762 near *MITF* contributes to the light skin color of the San. a, MPRA identified two MFVs in regulatory elements near *MITF*. Di-Ju, Di-Xoo and Di-San are Di-SNPs. The purple arrows indicate the direction of *MITF* gene transcription. The green tracks indicate ATAC-seq for MNT-1 and WM88, the blue tracks indicate ATAC-seq and ChIP–seq from normal human melanocytes (NHM) and the orange tracks indicate CUT&RUN from MNT-1. The black dashes are the Di-SNPs and the light-green shadowed regions represent enhancers E1 and E2. **b**,**c**, LRAs showed that rs111969762 located in E1 affects enhancer activity in both MNT-1 (**b**) and WM88 (**c**). Enhancers with T and C allele at rs111969762 are colored in green and orange, respectively. Two-tailed paired *t*-tests (MNT-1, $n = 6$; WM88, $n = 11$) were used. **d**, The chromatin interactions at the *MITF* locus, identified by Hi-C and H3K27ac HiChIP using Hae3 digestion. The upper matrix is from MNT-1 Hi-C data, and the lower matrix is from MNT-1 H3K27ac HiChIP data. TADs were called by onTAD and colored by nested TAD levels. The purple arches are loops called by cLoops. Melanocyte RNA-seq and DNase-seq tracks were downloaded from ENCODE[68]. The orange shadowed region represents enhancers E1. **e**, qPCR shows that CRISPRi of E1 significantly reduces the gene expression of *MITF*. A two-sided Dunnett's test with adjustments for multiple comparisons (control, $n = 8$; others, $n = 7$) was performed. **f**, CRISPRi of E1 significantly reduces melanin levels. Two-tailed unpaired *t*-tests (control, $n = 7$; MITF_E1_CRISPRi, $n = 8$) were performed. **g**, qPCR showed that CRISPR-mediated deletion of E1 significantly decreased the gene expression of *MITF*. Two-tailed unpaired *t*-tests ($n = 15$) were performed. **h**, CRISPR-mediated deletion of E1 significantly reduced melanin levels (two-tailed unpaired *t*-tests ($n = 8$) were performed). CRISPR was performed in MNT-1 using two sgRNAs. **i**, RNA-seq data showing differentially expressed genes in E1-deleted MNT-1. Genes plotted in this figure were selected using DESeq2 ($P < 0.05$, three biological replicates). **j**, Gene Ontology analysis of differentially expressed genes in E1-deleted MNT-1. Gene Ontologies related to pigmentation are colored in red. In panels **b**, **c**, **e**–**h**, different experimental groups are colored using different colors; the central vertical lines indicate the standard error of the mean; the *P* values are listed above the bars.

contributes to the relatively light skin color of the San by decreasing the enhancer activity and expression of *MITF*.

The role of Di-SNPs near *LEF1*, *TRPS1* and *BLOC1S6* in pigmentation

We further investigated other regulatory Di-SNPs that could potentially impact skin color in the San. These Di-SNPs include rs11939273 and rs17038630 near *LEF1*; rs75827647, rs10468581 and rs113940275 near *NLK*; rs11985280 near *TRPS1;* and rs72713175 near *BLOC1S6* (Fig. 5 and Extended Data Figs. 6–9). Based on MPRA and LRA, these Di-SNPs significantly affect the enhancer activity in MNT-1 or WM88 (Supplementary Table 5). Among all these SNPs, only rs17038630 near *LEF1*, rs11985280 near *TRPS1* and rs72713175 near *BLOC1S6* overlap open chromatin regions in MNT-1, WM88 and normal melanocytes (Fig. 5). Importantly, the *LEF1* locus is associated with hair color[39,40], the *TRPS1* locus is associated with sunburns[39] and tanning[41] and inactivating mutations in *BLOC1S6* cause reduced hair pigmentation in mice[42]. Thus, we further investigate the roles of these loci in pigmentation.

LEF1 is a transcription factor that regulates the expression of *MITF* and *TYR*[43,44]. Di-SNP rs17038630 is in the third intron of *LEF1* and its derived allele, rs17038630-T, is at higher frequency in the San (0.80) compared with other populations (<0.4, Fig. 5a,b). rs17038630-T is associated with decreased enhancer activity compared with rs17038630-G in both MNT-1 and WM88 (Fig. 5c,d and Extended Data Fig. 6b), consistent with the observation that the G-to-T mutation at rs17038630 disrupts the binding motif of LEF1 and SOX10 (Extended Data Fig. 6c). CRISPRi of enhancer E1 significantly reduced *LEF1* expression and melanin levels in MNT-1 ($P < 0.001$, Fig. 5e,f). However, CRISPR-KO of E1 did not significantly impact *LEF1* expression and melanin levels in MNT-1 (Extended Data Fig. 6e). We also identified three functional Di-SNPs near *NLK* by MPRA and LRA (Extended Data Fig. 7 and Supplementary Table 5). NLK is a serine/threonine protein kinase that phosphorylates LEF1[45,46] and is associated with sunburns[39]. In summary, we identified regulatory variants near *LEF1* and *NLK*, which may impact pigmentation.

TRPS1 is a transcription factor impacting the development of various tissues, including kidney, bone and hair follicles[47]. We observed that 161 Di-SNPs are located upstream of *TRPS1* and only rs11985280 overlaps a melanocyte-specific ATAC-seq peak (Fig. 5g and Extended Data Fig. 8a). The derived allele rs11985280-C is associated with decreased enhancer activity in both MNT-1 and WM88 (Fig. 5i,j and Extended Data Fig. 8b). Consistent with this observation, the T-to-C mutation at rs11985280 disrupts the binding motif of CCAAT/enhancer-binding proteins CEBPA/CEBPB (Extended Data Fig. 8c). CEBPA/CEBPB are downstream targets of STAT3, and loss of STAT3 enhances pigmentation[48]. CRISPRi of the enhancer containing rs11985280 significantly reduced the expression of *TRPS1* and melanin levels in MNT-1 (Fig. 5k,l). CRISPR-KO of the enhancer of *TRPS1* significantly decreased its expression but not the melanin level in MNT-1 (Extended Data Fig. 8d). Based on 180G (ref. 18) and SGDP[49] datasets, the San exhibit the highest frequency of rs11985280-C in Africa, with a frequency of 1.00 in Ju|'hoansi and 0.97 in !Xoo, followed by the relatively lightly pigmented Ethiopian Amhara population at 0.90. Furthermore, rs11985280-C is nearly fixed in the European (0.997), East Asian (0.997) and South Asian (0.983) populations based on the 1000G (ref. 31) dataset (Fig. 5h). In comparison, populations that are relatively more darkly pigmented, including the Baka, Chabu, Dizi, Fulani, Hadza, Herero, Mursi, Sandawe, Tikari and Oceanians, have a lower frequency ranging from 0.17 to 0.43 (Fig. 5h). Indeed, the F_{ST} value (Wright's fixation index) for CEU (Utah residents with Northern and Western European ancestry from the CEPH collection) versus YRI (Yoruba in Ibadan, Nigeria) (0.714) and CHB (Han Chinese in Beijing, China) versus YRI (0.725) rank in the top 0.05% and 0.1% across the genome, respectively. The GWAS-All dataset shows rs11985280-C is associated with light skin color ($P = 0.088$), although the association is not significant, possibly due to limited power because of lack of variability in the San and Amhara populations. However, the

Fig. 5 | Regulatory SNPs of *LEF1* and *TRPS1* contribute to the light skin color of the San. a, MPRA identified two MFVs near the *LEF1* locus. The purple arrows indicate the direction of *LEF1* gene transcription. The green tracks indicate ATAC-seq for MNT-1 and WM88, the blue tracks indicate ATAC-seq and ChIP–seq from NHM and the orange tracks indicate CUT&RUN from MNT-1. The black dashes are Di-SNPs, and the light green shadowed regions represent the locations of enhancers E1 and E2. **b**, The allele frequency at rs17038630 in global populations using data from the 1000G (ref. 31), African 5M (ref. 13) and SGDP[49] datasets. **c**,**d**, LRAs show that rs17038630 located in E1 affects enhancer activity in both MNT-1 (**c**) and WM88 (**d**). Two-tailed paired *t*-tests (MNT-1, $n = 6$; WM88, $n = 9$) were performed. **e**, qPCR showed that CRISPRi of E1 significantly reduces the gene expression of *LEF1*. A two-sided Dunnett's test with adjustments for multiple comparisons (control, $n = 17$; others, $n = 9$) was performed. **f**, CRISPRi of E1 significantly reduces melanin levels. A two-sided Dunnett's test with adjustments for multiple comparisons (control, $n = 18$; others, $n = 9$) was performed. **g**, MPRA identified one MFV near the *TRPS1* locus. The purple arrows indicate the direction of *TRPS1* gene transcription. **h**, The map shows the allele frequency at rs11985280 in global populations. The data are from the 180G (ref. 18), SGDP[49] and 1000G (ref. 31) datasets. **i**,**j**, LRAs showed that rs11985280 located in E1 affects enhancer activity in both MNT-1 (**i**) and WM88 (**j**). Two-tailed paired *t*-tests (MNT-1, $n = 9$; WM88, $n = 6$) were performed. **k**, qPCR showed that CRISPRi of the enhancer harboring rs11985280 significantly reduces the gene expression of *TRPS1*. A two-sided Dunnett's test with adjustments for multiple comparisons (control, $n = 11$; others, $n = 9$) was performed. **l**, CRISPRi of the enhancer harboring rs11985280 significantly reduces melanin levels. Two-tailed unpaired *t*-tests (control, $n = 18$; others, $n = 9$) were performed. In panels **c**–**f**, **i**–**l**, different experimental groups are colored using different colors; the central vertical lines indicate the standard error of the mean; the *P* values are listed above the bars.

https://doi.org/10.1038/s41588-023-01626-1

region encompassing *TRPS1* is significantly associated with skin color in the UKBB[7] dataset (leading SNP rs2721954; $P = 1.2 \times 10^{-91}$). Together, these results suggest that *TRPS1* plays a role in human skin pigmentation in global populations.

BLOC1S6 is involved in intracellular vesicle trafficking and melanosome biogenesis[50]. Using MPRA, we identified a Di-SNP—rs72713175—located 1 kb upstream of *BLOC1S6*, impacting the enhancer activity in WM88 (Extended Data Fig. 9a,b). The frequency of rs72713175-T, which

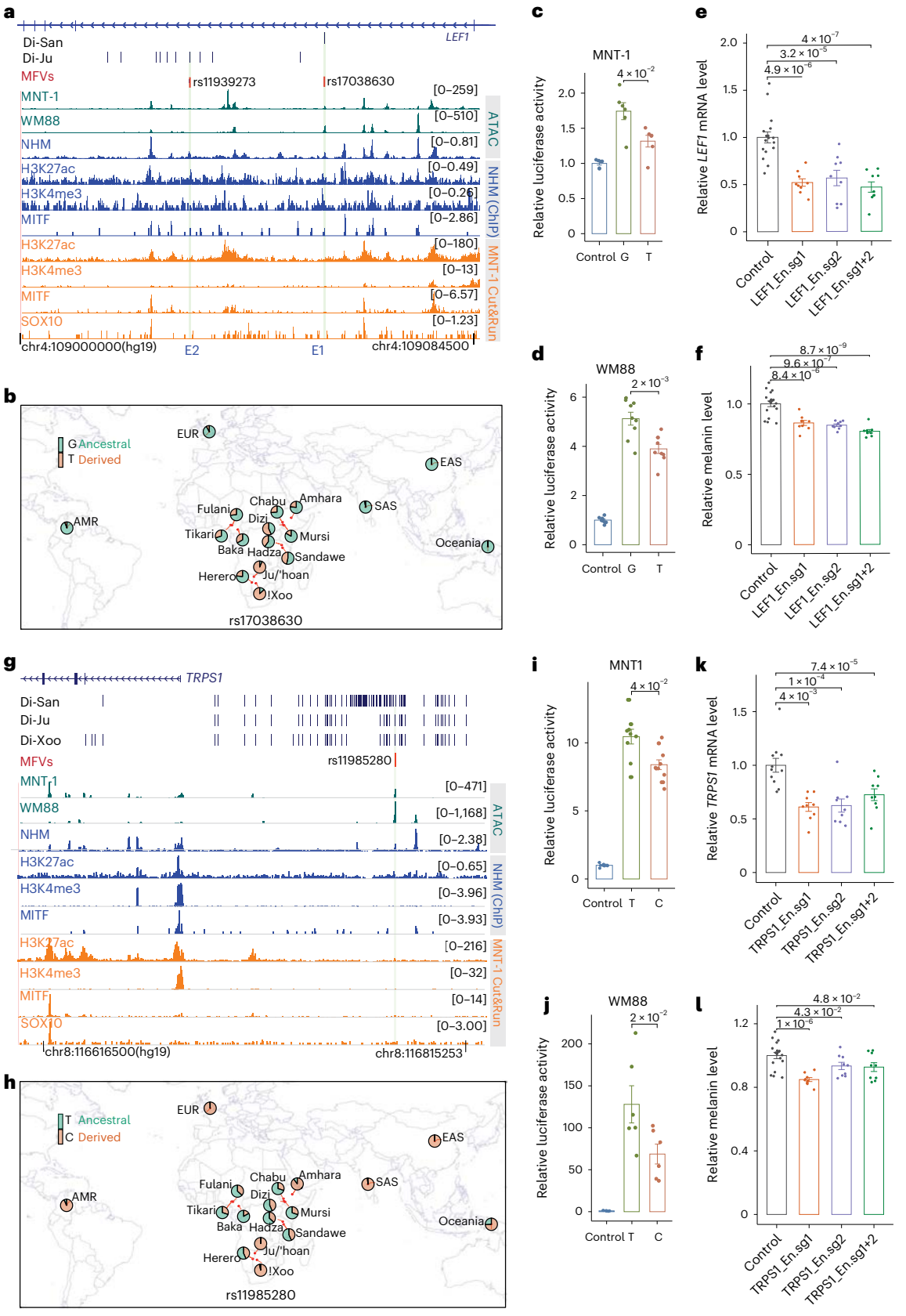

https://doi.org/10.1038/s41588-023-01626-1

is correlated with decreased enhancer activity, is much higher in the San (0.61) than in other populations (<0.31, Extended Data Fig. 9c). When we tested a 1.8 kb region (including rs72713175 and the promoter of *BLOC1S6*) using LRAs, rs72713175 did not significantly affect the enhancer activity in either MNT-1 or WM88, indicating that the effect of rs72713175 on gene expression is negligible relative to the effect of the promoter (Extended Data Fig. 9d). However, CRISPRi of this region significantly reduced *BLOC1S6* expression and pigmentation in MNT-1 (Extended Data Fig. 9e,f), suggesting that this SNP lies within a functional enhancer and that BLOC1S6 impacts pigmentation in human cells, consistent with the observation of decreased pigmentation in a mouse knockout model[42].

TMEM138 and *CYB561A3* are target genes of rs7948623

Previous studies reported that GWAS-SNP rs7948623 affects the activity of an enhancer interacting with the *DDB1* promoter and hypothesized

Fig. 6 | *CYB561A3* and *TMEM138* are the primary target genes of GWAS-SNP rs7948623. a, Three regulatory variants identified by MPRA near the *DDB1* locus. The purple arrows indicate the direction of gene transcription. The red dashes are MFVs, and the light green shadowed regions represent enhancers E1, E2 and E3. **b**, LRA shows that rs7948623 affects enhancer activity. Two-tailed paired *t*-tests for MNT-1 ($n = 9$) and WM88 ($n = 6$) were performed. **c**, The allele A at rs7948623 is associated with light skin color in Africans ($n = 1544$), and the *P* value was calculated using EPACTS 'q. emmax' method. **d**, Chromatin interactions near *DDB1* were identified by Hi-C and H3K27ac HiChIP. The light-green shadowed regions represent enhancers E1 and the interaction matrix between E1 and its targets were highlighted by orange triangles. The purple arches indicate loops identified by HiChIP. **e**, qPCR showed that CRISPRi of E1 in MNT-1 significantly decreases the expression of *CYB561A3* and *TMEM138* (two-sided Dunnett's test with adjustments for multiple comparisons (control sgRNA $n = 5$ and others $n = 3$)). **f**, qPCR shows that a CRISPR-mediated deletion of E1 significantly decreases the gene expression of *CYB561A3, TMEM138* and *DDB1*. Two-tailed unpaired *t*-tests without adjustments for multiple comparisons (in group No_sg (no sgRNA), TMEM138 ($n = 6$), CYB561A3 ($n = 12$), DDB1 ($n = 6$); in group Control_sg (control sgRNA), TMEM138 ($n = 6$), CYB561A3 ($n = 12$) and DDB1 ($n = 12$); in group E1_KO (E1 knockout), TMEM138 ($n = 5$), CYB561A3 ($n = 11$) and DDB1 ($n = 11$)) were performed. **g**, CRISPRi of E1 inhibits the gene expression of *CYB561A3* and *TMEM138* based on RNA-seq data. The top ten differentially expressed genes are labeled, and the *P* value was calculated by Wald's test with multiple testing correction in DESeq2. **h**, A volcano plot shows that CRISPR-mediated deletion of E1 reduces the gene expression of *CYB561A3* and *TMEM138*. The top ten differentially expressed genes are labeled and the *P* value was calculated by Wald's test with multiple testing correction in DESeq2. **i**, A Gene Ontology analysis of RNA-seq data shows CRISPRi of E1 affects the expression of genes in pigmentation-related pathways. **j**, A Gene Ontology analysis of RNA-seq data shows CRISPR-mediated deletion of E1 affects the expression of genes in pigmentation-related pathways. The data are presented as mean ± s.e.m. and an NS $P > 0.05$. In panels **b**, **e** and **f**, different experimental groups are colored using different colors; the central vertical lines indicate the standard error of the mean; the *P* values are listed above the bars. In panels **g** and **h**, red dots are genes with $|\log2FC| > 0.5$ and $P < 0.01$; blue dots are genes with $|\log2FC| < 0.5$ and $P < 0.01$; green dots are genes with $|\log2FC| > 0.5$ and $P > 0.01$; black dots are genes with $|\log2FC| < 0.5$ and $P > 0.01$. In panels **i** and **j**, Gene Ontologies related to pigmentation are highlighted in red.

that *DDB1* may impact skin color variation[13]. In this study, we use MPRA to study 17 GWAS-SNPs near *DDB1* and identified three MFVs (rs7948623 in E1, rs2277285 in E2 and rs2943806 in E3) in either MNT-1 or WM88 (Fig. 6a and Extended Data Fig. 10). Among the three MFVs, rs7948623 had the strongest association with skin color ($P = 1.42 \times 10^{-10}$ in GWAS-All) and showed the most significant allelic skew ($\log_2$FC −2.2, $P = 2.6 \times 10^{-118}$ in MNT-1; $\log_2$FC −0.2, $P = 2.3 \times 10^{-7}$ in WM88) as estimated by MPRA and validated by LRA (Fig. 6b and Extended Data Fig. 10b–d). The ancestral allele rs7948623-A, associated with lighter skin pigmentation, shows higher enhancer activity than the derived allele T (Fig. 6c), indicating that higher activity of E1 is associated with lighter skin pigmentation. Consistently, rs7948623 is located within a MITF binding site in melanocytes and mutation from A to T could disrupt the MITF binding motif (Fig. 6a and Extended Data Fig. 10e). SNPs rs2277285 and rs2943806 are in strong LD with each other ($R^2 = 0.89$) but are in moderate LD with rs7948623 ($R^2 = 0.62$, Extended Data Fig. 10f,g). Given that rs7948623 shows the strongest GWAS association and the highest allelic skew, further studies were focused on this SNP.

Using Hi-C and HiChIP, we detected interactions between the E1 enhancer containing rs7948623 and the promoters of *DDB1* (36.5 kb upstream of rs7948623), *CYB561A* and *TMEM138* (7.8 kb upstream of rs7948623), with the latter two promoters showing stronger interactions (Fig. 6d and Supplementary Fig. 24). CRISPRi or CRISPR-KO of E1 significantly decreased the expression of *TMEM138* and *CYB561A3* but had only minor effects on *DDB1* expression ($P > 0.1$ for CRISPRi and $P = 0.025$ for CRISPR-KO, Fig. 6e,f). RNA-seq of E1-inhibited MNT-1 confirmed that *TMEM138* and *CYB561A3* show the largest fold change among all transcribed genes ($\log_2$FC −1.27 and −1.27, respectively; Fig. 6g). Similarly, *TMEM138* and *CYB561A3* have the largest differences in gene expression in E1-deleted MNT-1 ($\log_2$FC −0.75 and −0.84, respectively; Fig. 6h). CYB561A3 (Cytochrome B561 family member A3) is an ascorbate-dependent ferrireductase in the lysosomal membrane[51] and is highly expressed in skin melanocytes[52] (transcripts per million (TPM) = 320, Supplementary Fig. 26). TMEM138 is a four-transmembrane domain protein involved in ciliary function[53] and is moderately expressed in skin melanocytes[52] (TPM = 37, Supplementary Fig. 26). Collectively, these results suggest that *CYB561A3* and *TMEM138* are the major target genes of rs7948623, and they may play a role in pigmentation.

CYB561A3 affects melanin levels in MNT-1 cells

Although neither CRISPRi nor CRISPR-KO of E1 significantly impacted melanin levels in MNT-1, both of them significantly affected the expression of known genes related to melanosome and melanogenesis pathways (Fig. 6i,j and Supplementary Fig. 25). Considering that deletion of E1 significantly reduces expression levels of *CYB561A3* and *TMEM138* (Fig. 6f,h) and that the allele at rs7948623 with higher enhancer activity is associated with lighter skin pigmentation (Fig. 6b,c), we hypothesized that decreasing the expression of CYB561A3/TMEM138 may enhance pigmentation. Indeed, overexpression of either CYB561A3 or TMEM138 in MNT-1 significantly reduced melanin levels in vitro (Fig. 7a

Fig. 7 | CYB561A3 affects melanin levels in MNT-1. a, Overexpression of CYB561A3 significantly decreases melanin levels in MNT-1. The top panel shows photos of pigmentation levels of MNT-1 on the bottom of a 24-well plate. The MNT-1 were first treated with 150 μM phenylthiourea (inhibits the biosynthesis of melanin) for 9 days and then infected with lentivirus encoding GFP, TMEM138–GFP, CYB561A3–GFP or CD63–GFP for 7 days. CD63–GFP is a negative control, which does not affect pigmentation. Different experimental groups are colored using different colors; the central vertical lines indicate the standard error of the mean. The *P* values were calculated using two-sided Tukey's test with adjustments for multiple comparisons ($n = 12$). **b**, The images show the confocal images of MNT-1 expressing CYB561A3–HA and immunostained with antibodies against the melanosomal marker TYRP1 (green) and HA (red). Scale bar, 10 μm. The bottom images represent the enlarged areas shown in blue boxes. The arrows point to regions of overlap (yellow) between CYB561A3–HA and TYRP1-positive cellular structures in three independent experiments. **c**, The graph shows the quantification of the overlap between CYB561A3–HA and TYRP1 in MNT-1 ($n = 10$ cells from three independent experiments). **d**, The volcano plot shows differentially expressed genes in CYB561A3-overexpressed MNT-1. The top ten most differentially expressed genes are labeled. The *P* value was calculated by Wald's test with multiple testing correction in DESeq2. **e**, KEGG pathway analysis shows overexpression of CYB561A3 affects the expression of genes related to mitochondrial respiration and melanin production. **f**, The overexpression of CYB561A3 affects the expression of genes related to melanosome and mitochondria function ($n = 3$). The genes involved in pigmentation were colored in black, and genes involved in mitochondrial function were colored in blue. **g**, A volcano plot of differentially expressed genes in *CYB561A3*-knockout MNT-1. The top ten differentially expressed genes are labeled, and the *P* value was calculated by Wald's test with multiple testing correction in DESeq2. **h**, A Gene Ontology analysis shows that *CYB561A3*-knockout affects melanogenesis-related pathways. **i**, Both knockout of *CYB561A3* and deletion of enhancer E1 affect the expression of genes related to melanin production. Listed genes have *P* values less than 0.05 based on DESeq2 ($n = 3$). For the boxplots in panels **f** and **i**, the central vertical lines are the median, with the boxes extending from the 25th to the 75th percentiles. The whiskers further extend by ±1.5 times the interquartile range from the limits of each box. The data are presented as mean ± s.e.m. In panels **d** and **g**, red dots are genes with $|\log2FC| > 0.5$ and $P < 0.01$; blue dots are genes with $|\log2FC| < 0.5$ and $P < 0.01$; green dots are genes with $|\log2FC| > 0.5$ and $P > 0.01$; black dots are genes with $|\log2FC| < 0.5$ and $P > 0.01$.

https://doi.org/10.1038/s41588-023-01626-1

and Supplementary Fig. 27), while the negative control CD63–GFP had no significant effects. Importantly, overexpression of CYB561A3 had a considerably larger impact on melanin levels compared with TMEM138 (log_2FC −2.2 versus −0.34, Fig. 7a) and did not affect cell proliferation in MNT-1 (Supplementary Fig. 27c).

To understand how CYB561A3 could regulate pigmentation, we investigated its subcellular localization using confocal imaging of immunostained HA-tagged human CYB561A3. In HeLa cells, CYB561A3–HA colocalized with the lysosomal protein LAMP1 (Supplementary Fig. 27d), as previously reported[51]. In MNT-1, however, a substantial fraction of CYB561A3–HA (79.45 ± 2.85%) colocalized with the TYRP1 protein found primarily in mature melanosomes (Fig. 7b,c), suggesting that CYB561A3 might regulate pigmentation.

To investigate the transcriptome-wide effects of CYB561A3, we performed RNA-seq of MNT-1 exogenously expressing CYB561A3 (Fig. 7d). Overexpression of CYB561A3 affects the expression of genes involved in mitochondrial respiration and melanin production (Fig. 7e,f and Supplementary Fig. 28). Notably, the gene most strongly downregulated in MNT-1-overexpressing CYB561A3 was *DCT* (log_2FC −1.1, $P = 1.1 \times 10^{-21}$, DESeq2, Fig. 7d,f), which encodes an enzyme critical for melanin biosynthesis. In addition, other genes that directly or indirectly regulate melanosome function, including *MC1R*, *PMEL* and *SLC45A2*, were also

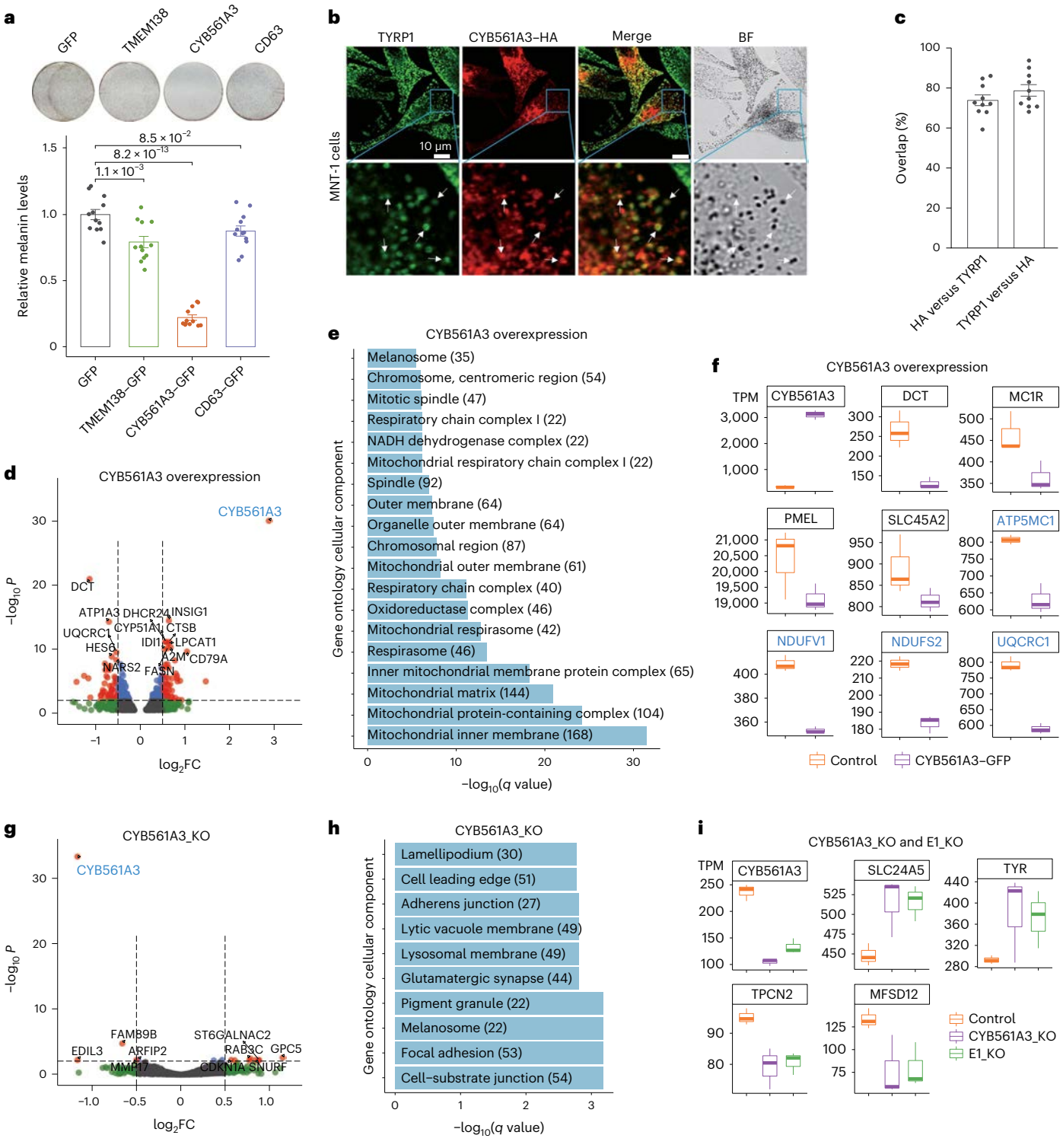

downregulated (Fig. 7f). Moreover, increased CYB561A3 expression also decreased the expression levels of genes related to mitochondrial function (Fig. 7f).

Similar to the deletion of the E1 enhancer of *CYB561A3* (Fig. 6), partial *CYB561A3* knockout (69%) had no significant effect on melanin levels in MNT-1, probably due to the already high levels of melanin in these cells (Supplementary Figs. 25c and 29). However, RNA-seq of these CRISPR-modified cells showed that decreased CYB561A3 significantly altered the expression of genes related to melanosome function in MNT-1 (Fig. 7g–i and Supplementary Fig. 30), consistent with the effects of the E1 deletion described above (Fig. 6j and Supplementary Fig. 25e). For example, *SLC24A5* and *TYR*, which positively regulate melanin production[54–56], were upregulated, whereas *MFSD12* and *TPCN2*, which negatively regulate melanin production[13,57], were downregulated in cells with reduced CYB561A3 mRNA. Taken together, we identified *CYB561A3* as a novel negative regulator of skin pigmentation.

Discussion

The San from Botswana have relatively light skin color compared with other African populations[5,13], possibly due to local adaptation, but the underlying genetic mechanism remains to be uncovered. We identified 77 Di-SNPs that are MFVs that alter enhancer activities in melanocyte-derived cells and validated the function of regulatory Di-SNPs near *MITF*, *LEF1*, *TRPS1* and *BLOC1S6* using LRA and CRISPR-based experiments. MITF, LEF1 and TRPS1 play important roles in the Wnt signaling pathway[45,46,58–61], regulating the development of melanocytes and hair[62,63]. Given that the San have relatively light skin color and a unique hair morphology compared with other African populations[18,64], these Di-SNPs may not only contribute to the light skin color of the San but also play a role in their hair phenotypes. These results shed light on the genetics and evolutionary history of light skin color in the San.

Most of the GWAS-SNPs and Di-SNPs (>98%) are located in noncoding regions, and SNPs in noncoding *cis*-regulatory elements could impact the expression of several genes, making it more difficult to directly determine the leading causal variants and their target genes[65]. Indeed, we discovered that the enhancer harboring rs6510760 affects the expression of *MFSD12* and *HMG20B*, both of which may impact pigmentation phenotypes: the enhancer harboring rs6497271 regulates the transcription of *OCA2* and *HERC2,* and the enhancer harboring rs7948623 affects the expression of *CYB561A3* and *TMEM138*, with a smaller effect on *DDB1*. These results revealed that one variant could affect multiple genes and, thus, have pleiotropic effects.

Human skin color variation is probably determined by hundreds of loci[4–13,66,67]. Inclusion of ethnically diverse and underrepresented populations in future genetic studies will be informative for identifying more loci underlying human skin pigmentation, as well as other variable phenotypes. In addition, since the causal variants/genes at most GWAS loci have not been confirmed, there is an urgent need for experimental validation. MPRA and CRISPR-based screens are promising high-throughput methods for transforming associations into causations, which will broaden our knowledge of complex traits and the treatment of human diseases.

Online content

Any methods, additional references, Nature Portfolio reporting summaries, source data, extended data, supplementary information, acknowledgments, peer review information; details of author contributions and competing interests; and statements of data and code availability are available at https://doi.org/10.1038/s41588-023-01626-1.

References

1. Jablonski, N. G. & Chaplin, G. Colloquium paper: human skin pigmentation as an adaptation to UV radiation. *Proc. Natl Acad. Sci. USA* **107**, 8962–8968 (2010).
2. Barsh, G. S. What controls variation in human skin color? *PLoS Biol.* **1**, E27 (2003).
3. Beleza, S. et al. Genetic architecture of skin and eye color in an African–European admixed population. *PLoS Genet.* **9**, e1003372 (2013).
4. Liu, F. et al. Genetics of skin color variation in Europeans: genome-wide association studies with functional follow-up. *Hum. Genet.* **134**, 823–835 (2015).
5. Martin, A. R. et al. An unexpectedly complex architecture for skin pigmentation in Africans. *Cell* **171**, 1340–1353 (2017).
6. Galván-Femenía, I. et al. Multitrait genome association analysis identifies new susceptibility genes for human anthropometric variation in the GCAT cohort. *J. Med. Genet.* **55**, 765–778 (2018).
7. Neale lab UK-Biobank GWAS result. *Neale Lab* http://www.nealelab.is/uk-biobank/ (2018).
8. Adhikari, K. et al. A GWAS in Latin Americans highlights the convergent evolution of lighter skin pigmentation in Eurasia. *Nat. Commun.* **10**, 358 (2019).
9. Lona-Durazo, F. et al. Meta-analysis of GWA studies provides new insights on the genetic architecture of skin pigmentation in recently admixed populations. *BMC Genet.* **20**, 59 (2019).
10. Jiang, L., Zheng, Z., Fang, H. & Yang, J. A generalized linear mixed model association tool for biobank-scale data. *Nat. Genet.* **53**, 1616–1621 (2021).
11. Batai, K. et al. Genetic loci associated with skin pigmentation in African Americans and their effects on vitamin D deficiency. *PLoS Genet.* **17**, e1009319 (2021).
12. Pairo-Castineira, E. et al. Expanded analysis of pigmentation genetics in UK Biobank. Preprint at *bioRxiv* https://doi.org/10.1101/2022.01.30.478418 (2022).
13. Crawford, N. G. et al. Loci associated with skin pigmentation identified in African populations. *Science* **358**, eaan8433 (2017).
14. Miller, C. T. et al. *cis*-Regulatory changes in KIT ligand expression and parallel evolution of pigmentation in sticklebacks and humans. *Cell* **131**, 1179–1189 (2007).
15. Tsetskhladze, Z. R. et al. Functional assessment of human coding mutations affecting skin pigmentation using zebrafish. *PLoS ONE* **7**, e47398 (2012).
16. Visser, M., Kayser, M. & Palstra, R.-J. HERC2 rs12913832 modulates human pigmentation by attenuating chromatin-loop formation between a long-range enhancer and the OCA2 promoter. *Genome Res.* **22**, 446–455 (2012).
17. Praetorius, C. et al. A polymorphism in IRF4 affects human pigmentation through a tyrosinase-dependent MITF/TFAP2A pathway. *Cell* **155**, 1022–1033 (2013).
18. Fan, S. et al. Whole-genome sequencing reveals a complex African population demographic history and signatures of local adaptation. *Cell* **186**, 923–939.e14 (2023).
19. Gordon, M. G. et al. lentiMPRA and MPRAflow for high-throughput functional characterization of gene regulatory elements. *Nat. Protoc.* **15**, 2387–2412 (2020).
20. Akey, J. M. et al. Tracking footprints of artificial selection in the dog genome. *Proc. Natl Acad. Sci. USA* **107**, 1160–1165 (2010).
21. Myint, L., Avramopoulos, D. G., Goff, L. A. & Hansen, K. D. Linear models enable powerful differential activity analysis in massively parallel reporter assays. *BMC Genomics* **20**, 209 (2019).
22. Adelmann, C. H. et al. MFSD12 mediates the import of cysteine into melanosomes and lysosomes. *Nature* **588**, 699–704 (2020).
23. Luecke, S. et al. The aryl hydrocarbon receptor (AHR), a novel regulator of human melanogenesis. *Pigment Cell Melanoma Res.* **23**, 828–833 (2010).

24. Kayser, M. et al. Three genome-wide association studies and a linkage analysis identify HERC2 as a human iris color gene. *Am. J. Hum. Genet.* **82**, 411–423 (2008).
25. Lona-Durazo, F. et al. A large Canadian cohort provides insights into the genetic architecture of human hair colour. *Commun. Biol.* **4**, 1253 (2021).
26. Simcoe, M. et al. Genome-wide association study in almost 195,000 individuals identifies 50 previously unidentified genetic loci for eye color. *Sci. Adv.* **7**, eabd1239 (2021).
27. Liang, Z. et al. BL-Hi-C is an efficient and sensitive approach for capturing structural and regulatory chromatin interactions. *Nat. Commun.* **8**, 1622 (2017).
28. Mumbach, M. R. et al. HiChIP: efficient and sensitive analysis of protein-directed genome architecture. *Nat. Methods* **13**, 919–922 (2016).
29. Bhattacharyya, S., Chandra, V., Vijayanand, P. & Ay, F. Identification of significant chromatin contacts from HiChIP data by FitHiChIP. *Nat. Commun.* **10**, 4221 (2019).
30. Ochoa, D. et al. Open Targets Platform: supporting systematic drug-target identification and prioritisation. *Nucleic Acids Res.* **49**, D1302–D1310 (2021).
31. The 1000 Genomes Project Consortium. A global reference for human genetic variation. *Nature* **526**, 68–74 (2015).
32. Albers, P. K. & McVean, G. Dating genomic variants and shared ancestry in population-scale sequencing data. *PLoS Biol.* **18**, e3000586 (2020).
33. Levy, C., Khaled, M. & Fisher, D. E. MITF: master regulator of melanocyte development and melanoma oncogene. *Trends Mol. Med.* **12**, 406–414 (2006).
34. Klein, J. C. et al. A systematic evaluation of the design and context dependencies of massively parallel reporter assays. *Nat. Methods* **17**, 1083–1091 (2020).
35. Tan, B. et al. FOXP3 over-expression inhibits melanoma tumorigenesis via effects on proliferation and apoptosis. *Oncotarget* **5**, 264–276 (2014).
36. Cao, Y. et al. Accurate loop calling for 3D genomic data with cLoops. *Bioinformatics* **36**, 666–675 (2020).
37. Takeda, K. et al. Induction of melanocyte-specific microphthalmia-associated transcription factor by Wnt-3a. *J. Biol. Chem.* **275**, 14013–14016 (2000).
38. Bondurand, N. et al. Interaction among SOX10, PAX3 and MITF, three genes altered in Waardenburg syndrome. *Hum. Mol. Genet.* **9**, 1907–1917 (2000).
39. Kichaev, G. et al. Leveraging polygenic functional enrichment to improve GWAS power. *Am. J. Hum. Genet.* **104**, 65–75 (2019).
40. Morgan, M. D. et al. Genome-wide study of hair colour in UK Biobank explains most of the SNP heritability. *Nat. Commun.* **9**, 5271 (2018).
41. Visconti, A. et al. Genome-wide association study in 176,678 Europeans reveals genetic loci for tanning response to sun exposure. *Nat. Commun.* **9**, 1684 (2018).
42. Larimore, J. et al. Mutations in the BLOC-1 subunits dysbindin and muted generate divergent and dosage-dependent phenotypes. *J. Biol. Chem.* **289**, 14291–14300 (2014).
43. Saito, H. et al. Melanocyte-specific microphthalmia-associated transcription factor isoform activates its own gene promoter through physical interaction with lymphoid-enhancing factor 1. *J. Biol. Chem.* **277**, 28787–28794 (2002).
44. Wang, X. et al. LEF-1 regulates tyrosinase gene transcription in vitro. *PLoS ONE* **10**, e0143142 (2015).
45. Ishitani, T. et al. The TAK1–NLK–MAPK-related pathway antagonizes signalling between β-catenin and transcription factor TCF. *Nature* **399**, 798–802 (1999).
46. Ishitani, T., Ninomiya-Tsuji, J. & Matsumoto, K. Regulation of lymphoid enhancer factor 1/T-cell factor by mitogen-activated protein kinase-related Nemo-like kinase-dependent phosphorylation in Wnt/β-catenin signaling. *Mol. Cell. Biol.* **23**, 1379–1389 (2003).
47. Gai, Z., Gui, T. & Muragaki, Y. The function of TRPS1 in the development and differentiation of bone, kidney, and hair follicles. *Histol. Histopathol.* **26**, 915–921 (2011).
48. Swoboda, A. et al. STAT3 promotes melanoma metastasis by CEBP-induced repression of the MITF pathway. *Oncogene* **40**, 1091–1105 (2021).
49. Mallick, S. et al. The Simons Genome Diversity Project: 300 genomes from 142 diverse populations. *Nature* **538**, 201–206 (2016).
50. Sitaram, A. & Marks, M. S. Mechanisms of protein delivery to melanosomes in pigment cells. *Physiology* **27**, 85–99 (2012).
51. Wang, Z. et al. CYB561A3 is the key lysosomal iron reductase required for Burkitt B-cell growth and survival. *Blood* **138**, 2216–2230 (2021).
52. Karlsson, M. et al. A single-cell type transcriptomics map of human tissues. *Sci. Adv.* **7**, eabh2169 (2021).
53. Lee, J. H. et al. Evolutionarily assembled *cis*-regulatory module at a human ciliopathy locus. *Science* **335**, 966–969 (2012).
54. Lamason, R. L. et al. SLC24A5, a putative cation exchanger, affects pigmentation in zebrafish and humans. *Science* **310**, 1782–1786 (2005).
55. Lavado, A., Olivares, C., García-Borrón, J. C. & Montoliu, L. Molecular basis of the extreme dilution mottled mouse mutation: a combination of coding and noncoding genomic alterations. *J. Biol. Chem.* **280**, 4817–4824 (2005).
56. Seruggia, D., Fernández, A., Cantero, M., Pelczar, P. & Montoliu, L. Functional validation of mouse tyrosinase non-coding regulatory DNA elements by CRISPR–Cas9-mediated mutagenesis. *Nucleic Acids Res.* **43**, 4855–4867 (2015).
57. Ambrosio, A. L., Boyle, J. A., Aradi, A. E., Christian, K. A. & Di Pietro, S. M. TPC2 controls pigmentation by regulating melanosome pH and size. *Proc. Natl Acad. Sci. USA* **113**, 5622–5627 (2016).
58. Ploper, D. et al. MITF drives endolysosomal biogenesis and potentiates Wnt signaling in melanoma cells. *Proc. Natl Acad. Sci. USA* **112**, E420–E429 (2015).
59. Zhang, Y. et al. Lef1 contributes to the differentiation of bulge stem cells by nuclear translocation and cross-talk with the Notch signaling pathway. *Int. J. Med. Sci.* **10**, 738–746 (2013).
60. Fantauzzo, K. A., Kurban, M., Levy, B. & Christiano, A. M. Trps1 and its target gene Sox9 regulate epithelial proliferation in the developing hair follicle and are associated with hypertrichosis. *PLoS Genet.* **8**, e1003002 (2012).
61. Fantauzzo, K. A. & Christiano, A. M. Trps1 activates a network of secreted Wnt inhibitors and transcription factors crucial to vibrissa follicle morphogenesis. *Development* **139**, 203–214 (2012).
62. Yamada, T. et al. Wnt/β-catenin and kit signaling sequentially regulate melanocyte stem cell differentiation in UVB-induced epidermal pigmentation. *J. Invest. Dermatol.* **133**, 2753–2762 (2013).
63. Andl, T., Reddy, S. T., Gaddapara, T. & Millar, S. E. WNT signals are required for the initiation of hair follicle development. *Dev. Cell* **2**, 643–653 (2002).
64. Tobias, P. V. & Biesele, M. *The Bushmen: San Hunters and Herders of Southern Africa* (Human & Rousseau, 1978).
65. Feng, Y., McQuillan, M. A. & Tishkoff, S. A. Evolutionary genetics of skin pigmentation in African populations. *Hum. Mol. Genet.* **30**, R88–R97 (2021).
66. Rawofi, L. et al. Genome-wide association study of pigmentary traits (skin and iris color) in individuals of East Asian ancestry. *PeerJ* **5**, e3951 (2017).

67. Stokowski, R. P. et al. A genomewide association study of skin pigmentation in a South Asian population. *Am. J. Hum. Genet.* **81**, 1119–1132 (2007).
68. ENCODE Project Consortium. An integrated encyclopedia of DNA elements in the human genome. *Nature* **489**, 57–74 (2012).

[1]Department of Genetics, University of Pennsylvania, Philadelphia, PA, USA. [2]Department of Bioengineering and Therapeutic Sciences, University of California San Francisco, San Francisco, CA, USA. [3]Institute for Human Genetics, University of California San Francisco, San Francisco, CA, USA. [4]Department of Neuroscience, Brown University, Providence, RI, USA. [5]Department of Biochemistry and Molecular Biology, Hubert Kairuki Memorial University, Dar es Salaam, Tanzania. [6]Department of Biological Sciences, Faculty of Sciences, University of Botswana, Gaborone, Botswana. [7]Department of Biomedical Sciences, University of Botswana, Gaborone, Botswana. [8]Department of Pharmacotoxicology and Pharmacokinetics, Faculty of Medicine and Biomedical Sciences, The University of Yaoundé I, Yaoundé, Cameroon. [9]Department of Biology, Addis Ababa University, Addis Ababa, Ethiopia. [10]Brain Research Africa Initiative (BRAIN); Neuroscience Lab, Faculty of Medicine and Biomedical Sciences, The University of Yaoundé I, Department of Neurology, Central Hospital Yaoundé, Yaoundé, Cameroon. [11]Department of Pathology and Laboratory Medicine, Children's Hospital of Philadelphia Research Institute, Philadelphia, PA, USA. [12]Department of Biology, University of Pennsylvania, Philadelphia, PA, USA. [13]Center for Global Genomics and Health Equity, University of Pennsylvania, Philadelphia, PA, USA. [14]Present address: Institute for the Advanced Study of Human Biology (WPI-ASHBi), Kyoto University, Kyoto, Japan. [15]Present address: Human Phenome Institute, School of Life Science, Fudan University, Shanghai, China.
✉e-mail: tishkoff@pennmedicine.upenn.edu

Methods

Samples and ethics

The collection of samples and data for this study conformed to all relevant ethical regulations. Before sample collection, we obtained permits from local institutions in Africa. An appropriate institutional review board approval was also obtained from the University of Pennsylvania. All individuals involved in this study have approved written informed consents. For the details of the sample information for the 5M SNP array data, see Crawford et al.[13]. For the details of sample information for the 180 WGS data, see Fan et al.[18]. The melanin index data were inferred using red reflectance values from skin in a minimally sun-exposed region (underside of the arm), as detailed in Crawford et al.[13].

Cell lines and cell culture

MNT-1 (ATCC, no. CRL- 3450), a gift from Dr. Michael S. Marks at the Children's Hospital of Philadelphia Research Institute, was grown in Dulbecco's modified Eagle medium (DMEM; Gibco, no.11965084) supplemented with 20% fetal bovine serum (FBS), 1% GlutaMAX (Gibco, no. 35050061), 1% nonessential amino acid supplement (Gibco, no. 10370021), 1% penicillin–streptomycin (Gibco, no. 15140122) and 10% AIM-V (Gibco, no. 12055-091).

WM88 (Rockland, no. WM88-01-0001), a melanocytic patient-derived melanoma tumor cell line, a gift from Dr. Ashani Weeraratna at the Wistar Institute, was cultured in Tumor Specialized medium (80% MCDB153, 20% Leibovitz's L-15, supplemented with 2% FBS and 1.68 mM CaCl2).

HeLa cells (CCL-2, ATCC) were cultured in DMEM supplemented with 10% FBS and 100 units ml^{-1} penicillin–streptomycin. Lenti-X 293T cells (Takara, no. 632180) were cultured in DMEM (Gibco, no. 11965084) supplemented with 10% FBS and 1% penicillin–streptomycin (Gibco, no. 15140122). All cells were cultured at 37 °C with 5% CO_2 in a humidified incubator.

Genome-wide association analysis

We conducted a genome-wide association analysis of skin color variation using 32,574,188 SNPs imputed from a previously published Illumina 5M SNP array dataset[13] of 1,544 GWAS-All samples. The SNPs were imputed using the following reference datasets: the 180 WGS[18] data were merged with SGDP[49] samples. Briefly, we imputed the 5M SNP array data[13] using Minimac3 and excluded SNPs with low quality (genotype quality score <0.3) and low frequency (MAF <0.00001 in the pooled dataset). The GWAS was conducted using a linear mixed model (EMMAX[69]) implemented in Efficient and Parallelizable Association Container Toolbox (EPACTS, v3.3.0)[70], and using kinship, sex, age and the top ten PCs as covariates. We also performed a GWAS for 500 individuals from Botswana (GWAS-Bots, which includes 314 San individuals and is a subset of the GWAS-All dataset) using the same software and parameters. The script used is: epacts single –vcf [input.vcf.gz]–ped [input.ped]–min-maf 0.01–kinf [input.kinf]–pheno [PHENO_NAME]–cov [COV1]–cov [COV2]–out [outprefix]–run [# of parallel jobs]–test q.emmax –anno. The association results were ranked on the basis of *P* values, and the top 4,999 SNPs were selected for downstream functional analysis.

Di analysis

To identify SNPs with highly differentiated allele frequencies between the relatively lightly pigmented San population (Ju|'hoan and !Xoo) and other African populations, we calculated the Di values for 9,413,188 variants from our 180G dataset (12 populations with 15 samples per population, Fan et al.[18]) and selected SNPs with the top 0.1% Di values for downstream functional analysis as described in Fan et al.[18]. The Di statistic is calculated using the following equation:

$$\mathrm{Di} = \sum_{j \neq i} (F_{ST}(i,j) - E[F_{ST}(i,j)])/\mathrm{sd}(F_{ST}(i,j))$$

,where $F_{ST}(i,j)$ is the Fst value at a SNP site between population i and j, $E[F_{ST}(i,j)]$ and $\mathrm{sd}[F_{ST}(i,j)]$ are the mean and standard deviation of F_{ST} values. F_{ST} measures the proportion of the genetic variance contained in a subpopulation relative to the genetic variance in all populations; S indicates the total genetic variance contained in a subpopulation; T indicates the total genetic variance contained in the total population. Values range from 0 to 1, with higher values indicating greater genetic differentiation between populations[71]. We performed three Di analyses: Ju|'hoan and !Xoo versus other populations (Di-San), Ju|'hoan versus other populations (excluding the !Xoo; Di-Ju) and !Xoo versus other populations (excluding the Ju|'hoan; Di-Xoo). SNP enrichment analyses were conducted using GREAT (V4.04)[72] and FUMA (V1.5.4)[73]. GREAT and FUMA calculate statistics by associating SNPs with their two nearest genes and using the genes as input for enrichment analysis.

SNP filtering and selection

We selected GWAS-SNPs for the MPRA located within melanocyte open chromatin regions (ATAC-seq/DNase sequencing (DNase-seq) peaks from melanoma cells and melanocytes) using the following 18 datasets from the ENCODE[68] and GEO[74] databases: GSM2476338, GSM2476339, GSM2476340, GSM2575295, GSM3083210, GSM774243, GSM1024610, GSM774244, GSM816631, GSM1027307, GSM1027312, GSM1014535, GSM1024793, GSM1024779, ENCFF560LQG, ENCFF600JNF, ENCFF862XVF and GSM1008599. We used GNU Wget v1.21.3 to download data from ENCODE. To select Di-SNPs related to skin pigmentation, we overlapped the top 0.1% Di-SNPs with melanocyte open chromatin regions as described above. We then focused on the Di-SNPs located within 1 Mb distance to the TSS of 760 candidate pigmentation-related genes. The 760 pigmentation-related genes were manually collected from three sources: 107 genes associated with pigmentation phenotypes in mice[75,76], 650 genes from a published review[77] and the top 100 genes highly expressed in the SK-MEL-30 cell line based on the protein atlas database[78].

LRA

The MNT-1 and WM88 cell lines were used for LRAs. The cells were plated in 24-well plates at 0.1 M per well, and 500 ng firefly luciferase plasmid, 20 ng pRL Renilla luciferase plasmid (Promega, no. E2231) and 1.5 µl Lipofectamine 3000 (Invitrogen, no. L3000150) were added to each well. After 36 h post-transfection, luciferase activity was determined using Dual-Luciferase Assay kit (Promega, no. E1910) according to the manufacturer's instructions. The luminescence signal was detected in a white 96-well plate using a SpectraMax i3x Multi-Mode Microplate reader. The reporter gene activity of firefly luciferase was normalized to that of Renilla luciferase to determine the activity of functional elements.

Plasmid cloning

For the luciferase reporter assays, human enhancer elements were cloned using genomic DNA extracted from MNT-1. The amplified enhancer fragments were sequenced and ligated to PGL4.23 vector (Promega, no. E8411) using the Gibson assembly (NEB, no. E2621). Candidate functional SNPs were introduced by mutated primers. For CRISPRi experiments, sgRNAs were designed by IDT[79] or CRISPOR (http://crispor.tefor.net/) and cloned into a pLKO5.sgRNA.EFS.GFP (Addgene, no. 57822) backbone vector using BsmBI. For CYB561A3 and TMEM138 cloning and expression, a pL-CRISPR.EFS.GFP (Addgene, no. 57818) plasmid was digested using Bamh1 and Nhe1, and the 7.5 kb fragment was gel extracted as the vector backbone. Human CYB561A3 and TMEM138 CDS were PCR amplified using cDNA from MNT-1. The CDS and vector (7.5 kb) fragments were assembled by Gibson assembly and transformed into Stbl3 competent cells. Plasmids were extracted using NucleoSpin Transfection-grade Kit (Takara, no. 740490.250) and sequenced to confirm the plasmid sequence. Oligo sequences are listed in Supplementary Table 8.

CRISPR knockout and inhibition

To perform enhancer CRISPR knockout or inhibition, we first constructed MNT-1 stable-expressing Cas9 (lentiCRISPR v2, Addgene, no. 52961) or dCas9-KRAB-MeCP2 (Addgene, no. 110821).

Then, we produced lentiCRISPR v2 (knockout) and dCas9–KRAB–MeCP2 (CRISPRi) lentiviruses following the published protocol[19]. Then, MNT-1 cells were infected with each virus with 8 μg ml^{-1} Polybrene (Sigma cat. no. H9268). For the knockout cell line, 24 h postinfection the medium was replaced using a full medium with puromycin (2 μg ml^{-1}, Gibco, no. A1113803), and the medium was changed every 24 h. After selection for 5 days, the MNT-1 cells were passaged to a 10-cm plate. The MNT-1-Cas9 cells were frozen for CRISPR-KO experiments. For the CRISPRi cell line, all procedures are similar except that the cells were selected with Blasticidin (5 μg ml^{-1}, Gibco, no. A1113903).

For CRISPR knockout of the enhancers, MNT-1 stable-expressing Cas9 cells were seeded in 24-well plates at a density of 0.05 M per well and cultured for 24 h. Then, the medium was changed to fresh medium with 8 μg ml^{-1} polybrene before infection. PLKO5-sgRNA (target-to-enhancer) viruses were added at ~10 multiplicity of infection, and the plates were centrifuged at 1,000*g* for 30 min at 32 °C. After 24 h postinfection, the medium was replaced using a full medium with puromycin (2 μg ml^{-1}) and changed every 24 h. The cells were collected for total RNA extraction or melanin assay 5 days after infection.

For enhancer CRISPRi, MNT-1 stable-expressing dCas9-KRAB-Mecp2 cells were seeded in 24-well plates at a density of 0.05 M per well and cultured for 24 h. The medium was changed to a fresh medium with 8 μg ml^{-1} polybrene (MNT-1) before infection. A PLKO5-sgRNA virus was added at ~10 multiplicity of infection, and the plates were centrifuged at 1,000*g* for 30 min at 32 °C. After 24 h postinfection, the medium was replaced using a full medium with blasticidin (5 μg ml^{-1}) and was changed every 24 h. Finally, the cells were collected for RNA extraction or melanin assays 5 days after infection.

RT–qPCR and RNA-seq

Total RNA was purified from all the cultured cells (CRISPR-KO, CRISPRi and overexpression) using Direct-zol RNA Miniprep Kits (Zymo, R2052) following the manufacturer's instructions, and the concentration was determined by a Nanodrop. For quantitative reverse transcription polymerase chain reaction (RT–qPCR), 200–500 ng of RNA was used for reverse transcription using a M-MLV Reverse Transcriptase (Promega, no. M1701) and Random Primer Mix (NEB, S1330). qPCR was conducted using Luna Universal qPCR Master Mix (NEB, M3003) on a QuantStudio 6 Flex Real-Time PCR machine (see Supplementary Table 8for primers). For RNA-seq, a total of 500 ng of RNA was sent to Genewiz to prepare sequencing libraries (see ref. 80 for details), Briefly, mRNA was selected by poly(A) enrichment, followed by fragmentation and reverse transcription, and addition of sequencing adapters and amplification. The final library was sequenced on Illumina HiSeq 2000 (150 bp paired-end sequences) at a depth of 20 million reads per library.

Immunostaining

Human CYB561A3 in pCMV-C–HA (Sino Biological, HG16893-CY) was transiently expressed in MNT-1 or HeLa cells using TransIT-LT1 Transfection Reagent (Mirus Bio) according to the manufacturer's instructions. Transfected cells on glass coverslips were fixed with 4% paraformaldehyde at room temperature for 15 min. Cells were incubated with 50 mM NH_4Cl for 10 min to quench free aldehyde groups, followed by incubation with blocking solution (0.2% saponin, 0.1% BSA and 0.02% sodium azide) containing primary antibodies for 1 h at room temperature. Following 4 × 5 min phosphate-buffered saline (PBS) washes, coverslips were incubated in fluorescently labeled secondary antibodies in blocking solution for 1 h at room temperature. Coverslips were washed with PBS for 5 min (four times) and inverted onto slides with ProLong Diamond Antifade Mountant. The antibodies used were mouse anti-TYRP1 (TA99/mel-5, 1:100, BioLegend), mouse anti-LAMP2 (H4A3, 1:20, Developmental Studies Hybridoma Bank) and rat anti-HA (ROAHAHA, 1:50, Roche). Host-specific secondary antibodies were conjugated to AlexaFluor 488 or 568 and used at a dilution of 1:1,000.

Confocal microscopy and image analysis

Images were acquired using an Olympus FV3000 laser scanning confocal microscope with a ×60 objective (1.3 NA; UPlan Super Apochromat). Colocalization analysis was performed using CellSens Dimension (v. 3.2). Briefly, each multichannel image was converted into an 8-bit image with a single channel. A region of interest (ROI) >10% of the cell surface area with low organelle density was selected for analysis. We generated binary images using the multiply channels operation and composite images were generated of two channels, where the total fluorescence of composite images was divided by the fluorescence of each single channel to calculate the percent overlap between channels.

Melanin assay

MNT-1 cells were washed with PBS twice and detached with 0.25% trypsin. The cells were pelleted at 300*g* for 3 min at room temperature, and the supernatant was removed gently. The cell pellet was washed once with PBS and lysed in 200 μl lysis buffer (50 mM Tris–HCl, pH 7.4, 2 mM EDTA, 150 mM NaCl and 1 mM dithiothreitol) per million cells. The lysis was vortexed three times every 5 min, and then spun down at 12,000*g* for 10 min at 4 °C. 50 μl supernatant was saved for protein quantification (BCA assay, Thermo Scientific, no.23225). Then, 150 μl 2× Protease Lysis buffer (20 mM Tris (pH 8), 200 mM NaCl, 50 mM EDTA, 1% SDS and 0.5 mg ml^{-1} proteinase K) was added to the rest lysate to digest the pellet. Pellets were rotated at 65 °C for 5 h and spun down at 12,000*g* for 10 min to collect melanin. The melanin pellets were dissolved in 0.45 ml of buffer N (2 M NaOH/20% dimethyl sulfoxide) and incubated at 60 °C for 30 min with shaking. Once melanin had fully dissolved (or if not, sonicated for 5 min), the melanin concentration was measured by absorbance at 450 nm. If necessary, the melanin was diluted so that the absorbance value was less than 0.35.

MPRA

We performed MPRA following the lentiMPRA[19] protocol with minor modifications (see Supplementary Notes 3 and 4 for details). The data analysis workflow was illustrated in Supplementary Fig. 4. Specifically, the paired-end 150 bp reads (R1 and R3) covering the 200 bp enhancer fragments were merged using Flash[81] (-m 50 -M 92). We obtained 98.6 million merged reads, of which 46.1% had the expected 200 bp length, 30.1% were 1 bp short and 11.7% were 2 bp short (short reads were excluded from downstream analysis). We extracted the 15-bp barcodes (R2) associated with each merged read and filtered out low-quality read pairs. At this step, we had 29.3 M high-quality read pairs (R1_R3_R2). We aligned the merged sequences to the reference enhancer sequences using BWA (bwa mem -t 4 -L 50 -k 10 -O 6 -B 5). To construct a unique enhancer-barcode dictionary, we removed repeated enhancer-barcode pairs and low-frequency pairs (<3 read pairs). We also filtered the pairs using the SAM-CIGAR string ($3 = = '200 M' && $4 = = 'MD:Z:200') to remove errors introduced by synthesizing and/or sequencing. The average barcode types per oligo are 126, and the average barcode count per oligo is 4,284 in the pre-library (Asso_Lib). In this library, there are 1,102 reference alleles, 1,103 alternative alleles, 148 negative controls and 30 positive controls. We sequenced the barcodes using paired-end 15 bp reads (r1 and r3) and merged them using Flash[81] (-m 15 -M 15). We filtered out low-quality read pairs (r1_r3_r2) using fastp[82] and removed PCR duplicates based on UMI. At this step, we have 66–74% reads remaining for barcode counting. We matched and counted the barcodes in the DNA and RNA libraries based on the enhancer-barcode associated library. Around 32% of the barcodes in the DNA and RNA libraries could be found in the association library.

We detected 1,099 ref–alt pairs (SNPs) in the DNA and RNA libraries. After obtaining the raw barcode counts from the DNA and RNA libraries, we performed allele-specific effect (ASE) analysis using the R package 'mpra'[21]. We prepared $K \times S$ integer matrices (K is the barcode count and S is the sample) and constructed a MPRASet object for both DNA and RNA libraries. We applied weighted linear models to test for differential enhancer activity using mpralm (TRUE for normalize and 'corr_groups' for model_type).

RNA-seq analysis

Raw RNA-seq fastq files were retrieved from the Genewiz server, and read quality was checked using FastQC[83]. Low-quality reads and adapters were filtered out using fastp[82] with default settings. Reference transcriptome (refMrna.fa.gz, hg38) and gene annotation (refGene.txt.gz, hg38) were downloaded from UCSC database. Transcript abundance was quantified by kallisto[84] with default settings. Gene level read counts were calculated using the Tximport package[85], and genes with mean read count less than ten were discarded. Differential expressed genes were identified using DESeq2 (ref. 86) and DEBrowser[87]. Differential expressed genes with an adjusted P value or an unadjusted P value less than 0.05 were selected for volcano plots using the EnhancedVolcano[88] package. A pathway enrichment analysis was performed using Pathview[89].

ATAC-seq

MNT-1 or WM88 cells were washed with PBS twice and detached with 0.25% trypsin. The cells were pelleted at 500*g* for 5 min at 4 °C, and the cell density was quantified by an Automated Cell Counter. Then, 50,000 viable cells were used for ATAC-seq following the Omni-ATAC protocol[90]. The Tn5 tagmentase was purchased from Diagenode (cat. no. C01070010).

Each ATAC-seq library was sequenced at a depth of >40 M paired-end reads by Nextseq 550. Then, the raw fastq files were filtered using fastp (v 0.22.0)[82] with default settings and mapped using bowtie2 (v 2.4.1)[91] with parameters '–very-sensitive–maxins 1000'. Duplicates and low-quality reads were removed using MarkDuplicates from gatk[92] (v 4.1.7.0) and samtools (v 1.13)[93] with parameters '-q 20 -F 1804 -f 2'. Bam files were converted to Bigwig files using deeptools2 (v 3.1.3)[94] with the setting '–normalizeUsing RPKM–binSize 10'. ATAC-seq peaks were called using macs2 (v 2.1.0.20150731)[95] with the setting 'callpeak -t in.bam -g hs -f BAMPE -q 0.01–keep-dup all'. The fraction of reads in peaks was calculated using the package featureCounts (v 2.0.3)[96]. TSS enrichment plots and correlation analysis were conducted using deeptools2[94].

CUT&RUN

MNT-1 cells were washed with PBS twice and detached with 0.25% trypsin. The cells were pelleted at 500*g* for 5 min at 4 °C and then fixed with 0.1% formaldehyde at room temperature for 1.5 min. Then, cells were quenched by adding 2.5 M glycine solution to a final concentration of 0.2 M. Finally, 500,000 cells were used for CUT&RUN using the CUT&RUN Kit (cat. no. 14-1048) from epicypher. The antibodies used for CUT&RUN include: MITF (CST, no. 97800), SOX10 (CST, no. 89356) and H3K27Ac (Abcam, no. ab4729). The H3K4me3 and IgG antibodies were from the CUT&RUN kit. All procedures were conducted following the manufacturer's manual.

Each CUT&RUN library was sequenced at a depth of >8 M paired-end reads by Nextseq 550. First, H3K4me3 antibody specificity was determined using the SNAP-CUTANA K-MetStat Panel. Second, the raw fastq files were filtered using fastp (v 0.22.0)[82] with default settings and mapped using bowtie2 (v 2.4.1)[91] with parameters '–dovetail–very-sensitive-local -I 10 -X 700'. The duplicates and low-quality reads were removed using MarkDuplicates from gatk[92] (v 4.1.7.0) and samtools (v 1.13)[93] with parameters '-q 20 -F 1804 -f 2'. Bam files were converted to Bedgraph and normalized using scale factors determined by spike-in Ecoli reads. Bam files were also converted to Bigwig files using deeptools2 (v 3.1.3)[94] with the setting '–normalizeUsing RPKM–binSize 10'. The H3K27ac CUT&RUN peaks were called using macs2 (v 2.1.0.20150731)[95] with the setting 'callpeak -t in.bam -g hs–broad–broad-cutoff 0.05 -f BAMPE–keep-dup all'. MITF, SOX10 and H3K4me3 CUT&RUN peaks were called using SEACR (v 1.3)[97]. The fraction of reads in peaks was calculated using the package featureCounts (v 2.0.3)[96]. TSS enrichment and correlation were conducted using deeptools2[94].

Transcription factor binding analysis

We used 'motifbreakR'[98] (v2.14.2) to predict the potential transcription factor binding motifs near functional SNPs. Briefly, we first transformed the SNP identification to Granges using the 'snps.from.rsid' function. Then, we used motifs from the hocomoco database[99] to predict effects for candidate variants. We visualized the candidate broken motifs using the plotMB function.

Identification of SNP–gene pairs by TAD and loops

To identify the SNPs and their potential target genes in the same TAD, we intersected the SNPs with all TADs called by onTAD[100] from all Hi-C experiments (see Supplementary Notesfor details). Then, we intersected the TADs with transcription start sites (TSS) from all human genes. We paired SNPs and genes that are in the same TAD. To identify the SNPs and their potential target genes by Hi-C or H3K27ac HiChIP loops, we extended the SNPs and TSSs to 2-kb fragments (SNP/TSS ± 1 kb). Then, we intersected the anchors of loops with these 2 kb bins and paired the SNPs and TSSs located in the anchors of the same loop.

Statistics and reproducibility

No statistical method was used to determine the sample size in advance. No data were excluded from the analyses. We randomly selected controls for MPRA. For confocal images and related quantification of MNT-1 cells, the cells were randomly selected. Other experiments were not randomized. The investigators were not blinded to allocation during the experiments and outcome assessment.

Additionally, a two-sided paired t-test was utilized to compare the means of the two groups in LRAs. A two-sided unpaired t-test was applied to compare the means of the two groups with unpaired data, specifically in CRISPRi and CRISPR-KO assays. When comparing the means among more than two groups, we initially conducted a one-way analysis of variance. Subsequently, we performed a two-sided Tukey's test with adjustments for multiple comparisons or a two-sided Dunnett's test with adjustments for multiple comparisons (with control group). In the case of MPRA, the P values were estimated using a random effects model for mpralm[21], and paired t-tests were conducted with multiple testing adjustments.

Reporting summary

Further information on research design is available in the Nature Portfolio Reporting Summary linked to this article.

Data availability

The epigenomic data, Hi-C and HiChIP data were uploaded to UCSC browser and are available at https://genome.ucsc.edu/s/fengyq/Tishkoff_Lab%2Dhg38%2DMPRA%2DHiC_Pigmentation. All RNA-seq and epigenomic data generated in this study are available at GEO GSE240717. Genotype data for GWAS are in dbGaP phs001396.vl.pl. Source data are provided with this paper.

Code availability

Public software and packages were used following the developer's manuals. The custom code used for data analysis has been deposited at GitHub (https://github.com/fengyq/nature_gentics_codes) and Zenodo[101] (https://zenodo.org/records/10198223).

References

69. Kang, H. M. et al. Variance component model to account for sample structure in genome-wide association studies. *Nat. Genet.* **42**, 348–354 (2010).
70. Kang, H. M. et al. Efficient and parallelizable association container toolbox, EPACTS v3.3.0. *EPACTS* http://genome.sph.umich.edu/wiki/EPACTS (2013).
71. Bhatia, G., Patterson, N., Sankararaman, S. & Price, A. L. Estimating and interpreting FST: the impact of rare variants. *Genome Res.* **23**, 1514–1521 (2013).
72. McLean, C. Y. et al. GREAT improves functional interpretation of *cis*-regulatory regions. *Nat. Biotechnol.* **28**, 495–501 (2010).
73. Watanabe, K., Taskesen, E., van Bochoven, A. & Posthuma, D. Functional mapping and annotation of genetic associations with FUMA. *Nat. Commun.* **8**, 1826 (2017).
74. Barrett, T. et al. NCBI GEO: mining millions of expression profiles—database and tools. *Nucleic Acids Res.* **33**, D562–D566 (2005).
75. Phenotype: pigmentation phenotype. *International Mouse Phenotyping Consortium* https://www.mousephenotype.org/data/phenotypes/MP:0001186 (2023)
76. Dickinson, M. E. et al. High-throughput discovery of novel developmental phenotypes. *Nature* **537**, 508–514 (2016).
77. Baxter, L. L., Watkins-Chow, D. E., Pavan, W. J. & Loftus, S. K. A curated gene list for expanding the horizons of pigmentation biology. *Pigment Cell Melanoma Res.* **32**, 348–358 (2019).
78. Uhlen, M. et al. A pathology atlas of the human cancer transcriptome. *Science* **357**, eaan2507 (2017).
79. Custom Alt-R™ CRISPR–Cas9 guide RNA. *Integrated DNA Technologies* https://www.idtdna.com/site/order/designtool/index/CRISPR_CUSTOM (2023).
80. RNA sequencing frequently asked questions. *GENEWIZ* https://web.genewiz.com/rna-seq-faq (2023).
81. Magoč, T. & Salzberg, S. L. FLASH: fast length adjustment of short reads to improve genome assemblies. *Bioinformatics* **27**, 2957–2963 (2011).
82. Chen, S., Zhou, Y., Chen, Y. & Gu, J. fastp: an ultra-fast all-in-one FASTQ preprocessor. *Bioinformatics* **34**, i884–i890 (2018).
83. FastQC. *GitHub* https://github.com/s-andrews/FastQC (2020)
84. Bray, N. L., Pimentel, H., Melsted, P. & Pachter, L. Near-optimal probabilistic RNA-seq quantification. *Nat. Biotechnol.* **34**, 525–527 (2016).
85. Soneson, C., Love, M. I. & Robinson, M. D. Differential analyses for RNA-seq: transcript-level estimates improve gene-level inferences. *F1000Res.* **4**, 1521 (2015).
86. Love, M. I., Huber, W. & Anders, S. Moderated estimation of fold change and dispersion for RNA-seq data with DESeq2. *Genome Biol.* **15**, 550 (2014).
87. Kucukural, A., Yukselen, O., Ozata, D. M., Moore, M. J. & Garber, M. DEBrowser: interactive differential expression analysis and visualization tool for count data. *BMC Genomics* **20**, 6 (2019).
88. Blighe, K., Rana, S., Lewis, M. EnhancedVolcano: publication-ready volcano plots with enhanced colouring and labeling. R package version 1.14.0. *EnhancedVolcano* https://github.com/kevinblighe/EnhancedVolcano (2023).
89. Luo, W. & Brouwer, C. Pathview: an R/Bioconductor package for pathway-based data integration and visualization. *Bioinformatics* **29**, 1830–1831 (2013).
90. Corces, M. R. et al. An improved ATAC-seq protocol reduces background and enables interrogation of frozen tissues. *Nat. Methods* **14**, 959–962 (2017).
91. Langmead, B. & Salzberg, S. L. Fast gapped-read alignment with Bowtie 2. *Nat. Methods* **9**, 357–359 (2012).
92. McKenna, A. et al. The genome analysis toolkit: a MapReduce framework for analyzing next-generation DNA sequencing data. *Genome Res.* **20**, 1297–1303 (2010).
93. Li, H. et al. The sequence Alignment/Map format and SAMtools. *Bioinformatics* **25**, 2078–2079 (2009).
94. Ramírez, F. et al. deepTools2: a next generation web server for deep-sequencing data analysis. *Nucleic Acids Res.* **44**, W160–W165 (2016).
95. Zhang, Y. et al. Model-based analysis of ChIP–seq (MACS). *Genome Biol.* **9**, R137 (2008).
96. Liao, Y., Smyth, G. K. & Shi, W. featureCounts: an efficient general purpose program for assigning sequence reads to genomic features. *Bioinformatics* **30**, 923–930 (2014).
97. Meers, M. P., Tenenbaum, D. & Henikoff, S. Peak calling by Sparse Enrichment Analysis for CUT&RUN chromatin profiling. *Epigenet. Chromatin* **12**, 42 (2019).
98. Coetzee, S. G., Coetzee, G. A. & Hazelett, D. J. motifbreakR: an R/Bioconductor package for predicting variant effects at transcription factor binding sites. *Bioinformatics* **31**, 3847–3849 (2015).
99. Kulakovskiy, I. V. et al. HOCOMOCO: towards a complete collection of transcription factor binding models for human and mouse via large-scale ChIP–seq analysis. *Nucleic Acids Res.* **46**, D252–D259 (2018).
100. An, L. et al. OnTAD: hierarchical domain structure reveals the divergence of activity among TADs and boundaries. *Genome Biol.* **20**, 282 (2019).
101. Feng, Y. Codes for skin pigmentation paper. *Zenodo* https://doi.org/10.5281/zenodo.10198223 (2023).
102. Shin, J. H., Blay, S., Graham, J. & McNeney, B. LDheatmap: an R function for graphical display of pairwise linkage disequilibria between single nucleotide polymorphisms. *J. Stat. Softw.* **16**, 1–9 (2006).
103. Liu, T. et al. Cistrome: an integrative platform for transcriptional regulation studies. *Genome Biol.* **12**, R83 (2011).

Acknowledgements

This research was supported by the following grants: NIH grants R35 GM134957-01, 3UM1HG009408-02S1, 1R01GM113657-01 and 5R01AR076241-02. We thank the Skin Biology and Disease Resource-based Center (SBDRC, NIH P30-AR069589) at the University of Pennsylvania for funding and providing human primary melanocytes. The sequencing of MPRA was carried out by the DNA Technologies and Expression Analysis Core at the University of California Davis Genome Center, supported by the NIH Shared Instrumentation Grant 1S10OD010786-01. We thank E. Burton for assistance on part of the plasmid cloning. We thank Z. (J.) Zhou from the Department of Genetics at the University of Pennsylvania for sharing their tissue culture room. We thank J. Phillips-Cremins from the Department of Genetics at the University of Pennsylvania for constructive suggestions on Hi-C. We thank H. Wong and H. Wu at the University of Pennsylvania for sharing their experimental equipment. We thank the African participants for their contributions to this study.

Author contributions

Y.F. and S.A.T. designed the study and wrote the original draft. Y.F. performed the Hi-C, H3K27ac HiChIP, CRISPR, RNA-seq, ATAC-seq and CUT&RUN experiments and related data analysis. Y.F. and F.I. conducted the MPRA under supervision of N.A. Y.F. and C.Z. analyzed the MPRA data. S.F. and M.E.B.H played a role in quality control and analysis of WGS and SNP array data. Y.F. and S.F. conducted the GWAS and Di analysis. Y.F. and N.X. performed CRISPR editing and related assays in MNT-1. S.A.T., T.N., S.W.M., G.G.M., A.K.N., C.F. and G.B. played a role in collecting data from Africa. J.S. and E.O. performed the CYB561A3 immunofluorescence imaging and analyses. E.O. and M.S.M. provided resources and additional experimental insights. All authors assisted with manuscript review and editing. S.A.T. supervised the project.

Competing interests

N.A. is an equity holder of Encoded Therapeutics, a gene regulation therapeutics company and is a cofounder and scientific advisor of

Regel Therapeutics and Neomer Diagnostics. The remaining authors declare no competing financial interests.

Additional information

Extended data is available for this paper at https://doi.org/10.1038/s41588-023-01626-1.

Supplementary information The online version contains supplementary material available at https://doi.org/10.1038/s41588-023-01626-1.

Correspondence and requests for materials should be addressed to Sarah A. Tishkoff.

Peer review information *Nature Genetics* thanks the anonymous reviewers for their contribution to the peer review of this work.

https://doi.org/10.1038/s41588-023-01626-1

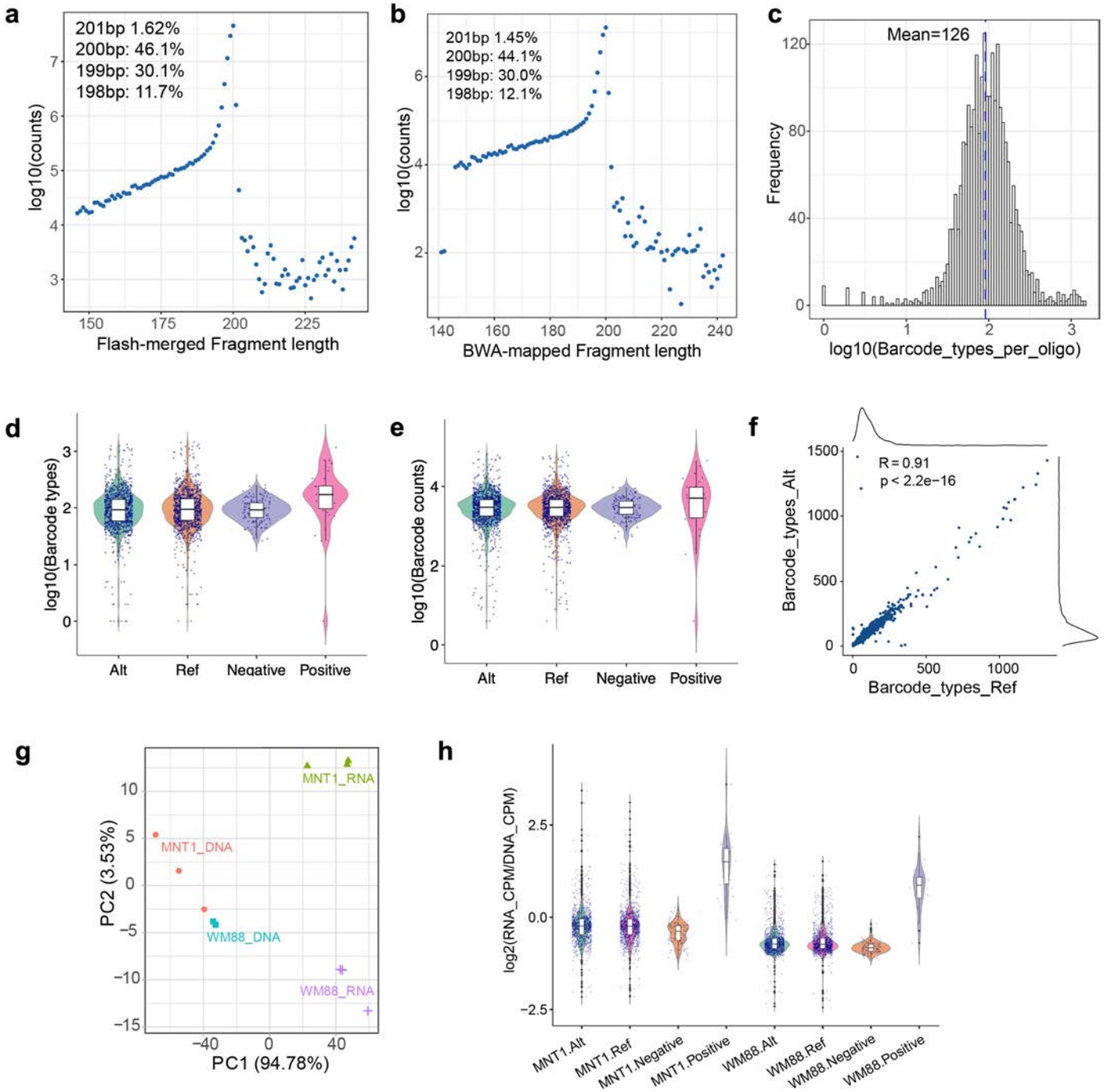

Extended Data Fig. 1 | Quality statistics of the MPRA experiments. (**a**) Statistics for FLASH-merged reads in the association library. The plot shows that 46.1% are 200 bp fragments as designed. (**b**) Statistics of BWA-mapped reads in the association library. The plot shows that 44.1% are 200 bp fragments as designed. (**c**) Statistics of barcode types per oligo in the association library. On average, each oligo is linked with 126 different barcodes. (**d**) Statistics of barcode types per oligo in reference (n = 1102), alternative (n = 1103), negative control (n = 153), and positive control (n = 30) oligos. Data is from the association library. (**e**) Statistics of barcode counts per oligo in reference (n = 1102), alternative (n = 1103), negative control (n = 153), and positive control (n = 30) oligos. Data is from the association library. (**f**) Barcode types for reference and alternative alleles are comparable. Pearson's r = 0.91, $p < 2 \times 10^{-16}$. (**g**) Principal component analysis of DNA and RNA libraries from MNT-1 and WM88 cells. Three replicates. (**h**) Summary of enhancer activities estimated by MPRA. Enhancer activities were defined as the barcode counts per million in the RNA library divided by the barcode counts per million in the DNA library. Alt: oligos containing alternative alleles (n = 1103). Ref: oligos containing reference alleles (n = 1102). Negative, negative control oligos (n = 148). Positive, positive control oligos (n = 30). For boxplots, central lines are median, with boxes extending from the 25th to the 75th percentiles. Whiskers further extend by ±1.5 times the interquartile range from the limits of each box.

https://doi.org/10.1038/s41588-023-01626-1

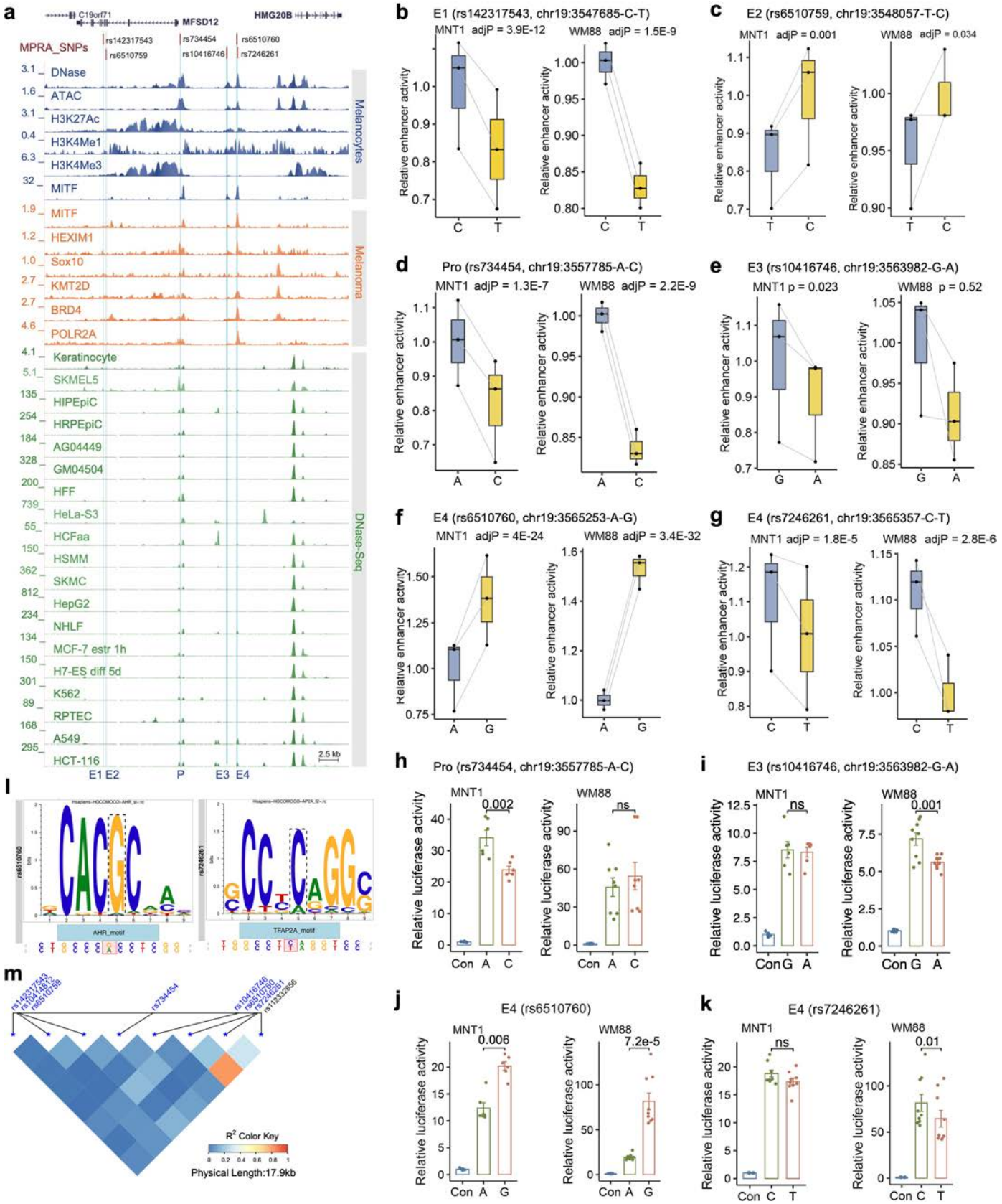

Extended Data Fig. 2 | See next page for caption.

https://doi.org/10.1038/s41588-023-01626-1

Extended Data Fig. 2 | MPRA identifies six allelic skewed variants near *MFSD12*. (**a**) Plot showing allelic skewed variants in regulatory regions near *MFSD12*. Blue tracks indicate DNase-Seq, ATAC-Seq, and ChIP-Seq from melanocytes; orange tracks indicate ChIP-Seq from melanoma (501-mel) cells; green tracks indicate DNase-Seq from ENCODE cell lines. E1-E4, enhancers. P, promoter. (**b**-**g**) Relative enhancer activities of the two alleles at rs142317543, rs6510759, rs734454, rs10416746, rs6510760, rs7246261 estimated by MPRA (n = 3). For b, c, d, f, g, p-values were estimated with a random effects model for mpralm and paired t-tests with multiple testing adjustments; e was without multiple testing adjustments. (**h**-**k**) Relative enhancer activities estimated by LRA. Two-tailed paired t-tests (For LRA in MNT1, n = 6. For LRA in WM88, 2 h n = 8; others n = 9). Data were presented as mean ± SEM. ns p > 0.05. (**l**) rs6510760 and rs7246261 disrupt the binding motifs of AHR and TFAP2, respectively. Predicted by 'MotifBreakR'[98]. (**m**) The LD pattern of candidate functional variants near *MFSD12*. LD was calculated using the 180 G[18] data by the LDheatmap[102] package. For boxplots, central lines are median, with boxes extending from the 25th to the 75th percentiles. Whiskers further extend by ±1.5 times the interquartile range from the limits of each box.

https://doi.org/10.1038/s41588-023-01626-1

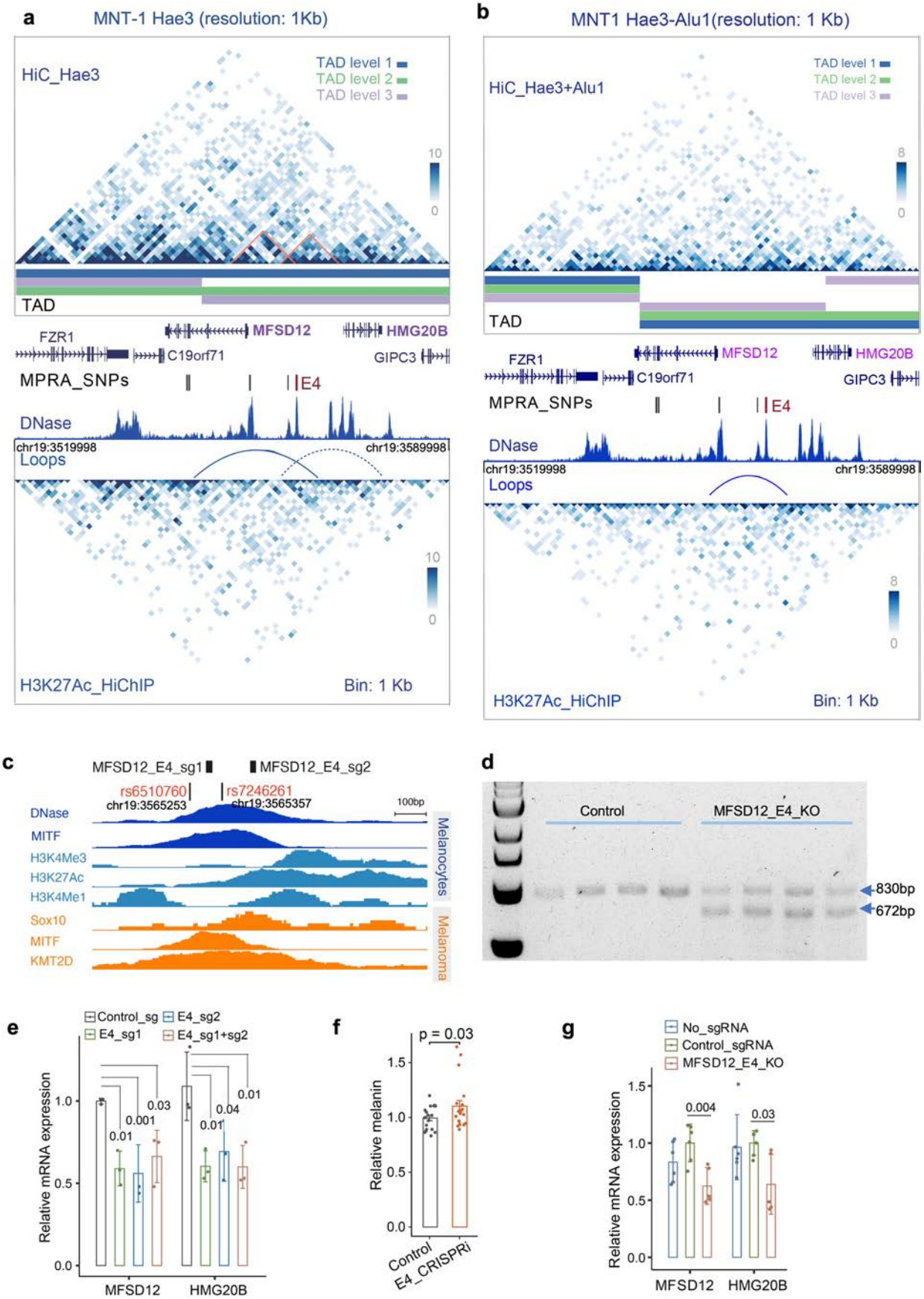

Extended Data Fig. 3 | See next page for caption.

https://doi.org/10.1038/s41588-023-01626-1

Extended Data Fig. 3 | The enhancer E4 interacts with the promoter of *MFSD12* and affects the expression of *MFSD12*. (**a**, **b**) Chromatin interactions near *MFSD12* identified by Hi-C and H3K27ac HiChIP with Hae3 digestion. The upper matrix is from MNT-1 Hi-C data, and the lower matrix is from MNT-1 H3K27ac HiChIP data. TADs were called by onTAD[100] and colored by nested TAD levels. The solid arch was a loop defined using FitHiChIP[29] software, the dashed arch was a potential loop based on the observed interaction matrix. The interaction matrix between *MFSD12* and *HMG20B* was highlighted with orange angles. The DNase track of melanocytes was downloaded from ENCODE[68]. rs6510760 and rs657246261 in E4 were colored in red. The plotted region is chr19:3519998-3589998 (hg19). (**c**) Schematic showing the location of the two sgRNAs targeting the enhancer E4 of *MFSD12*. (**d**) PCR results showing efficient knockout of the enhancer by the two sgRNAs. Three independent experiments. (**e**) qPCR showed that CRISPRi of E4 reduces the gene expression of *MFSD12* and *HMG20B* in MNT-1 cells. Two-sided Dunnett's test with adjustments for multiple comparisons (n = 3). (**f**) CRISPRi of E4 slightly increases melanin levels in MNT-1 cells. Two-tailed unpaired t-tests (n = 19). (**g**) qPCR showed that CRISPR knockout of E4 decreases the gene expression of *MFSD12* and *HMG20B* in MNT-1 cells. Two-tailed unpaired t-tests without multiple testing adjustments (n = 6). Data are presented as mean ± SEM.

https://doi.org/10.1038/s41588-023-01626-1

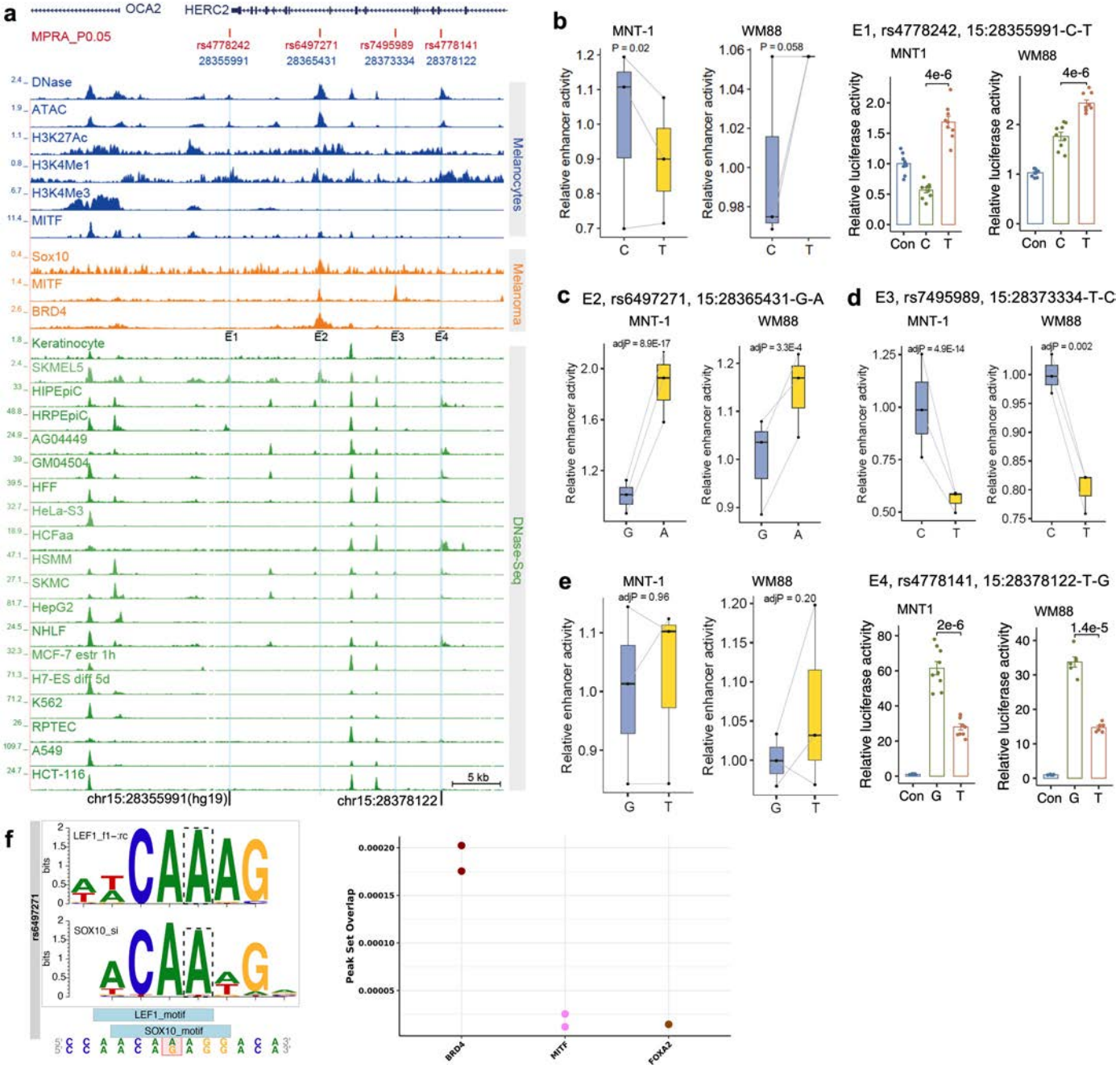

Extended Data Fig. 4 | Identification of functional variants associated with skin pigmentation near *OCA2*. (**a**) SNP rs6497271 is in a melanocyte-specific enhancer. Blue tracks indicate DNase-Seq, ATAC-Seq, and ChIP-Seq data from melanocytes; orange tracks indicate ChIP-Seq data from melanoma (501-mel) cells; green tracks indicate DNase-Seq data from ENCODE cell lines. E1-E4, enhancers. The plotted region is chr15: 28,335,146-28,385,146 (hg19). (**b**) MPRA and LRA reveals that rs4778242 significantly affects the enhancer activity of E1 in MNT-1 and WM88 cells. MPRA (n = 3), LRA (n = 9). (**c**) MPRA showed that rs6497271 affects the enhancer activity of E2 in MNT-1 and WM88 cells (n = 3). (**d**) MPRA shows that rs7495989 affects the enhancer activity of E3 in MNT-1 and WM88 cells (n = 3). (**e**) MPRA and LRA reveals that rs4778141 affects the enhancer activity of E4 in MNT-1 and WM88 cells. MPRA (n = 3), LRA (MNT-1, n = 9; WM88, n = 6). (**f**) rs6497271 overlaps transcription factor binding sites. Left panel shows rs6497271 disrupts the binding motif of LEF1 and SOX10. Right panel shows that rs6497271 overlaps ChIP-seq peaks from Cistrome database[103]. LRA data are presented as mean ± SEM, tested with two-tailed paired t-tests. MPRA p-values are estimated with a random effects model for mpralm and paired t-tests with multiple testing adjustments. For MPRA boxplots, central lines are median, with boxes extending from the 25th to the 75th percentiles. Whiskers further extend by ±1.5 times the interquartile range from the limits of each box.

https://doi.org/10.1038/s41588-023-01626-1

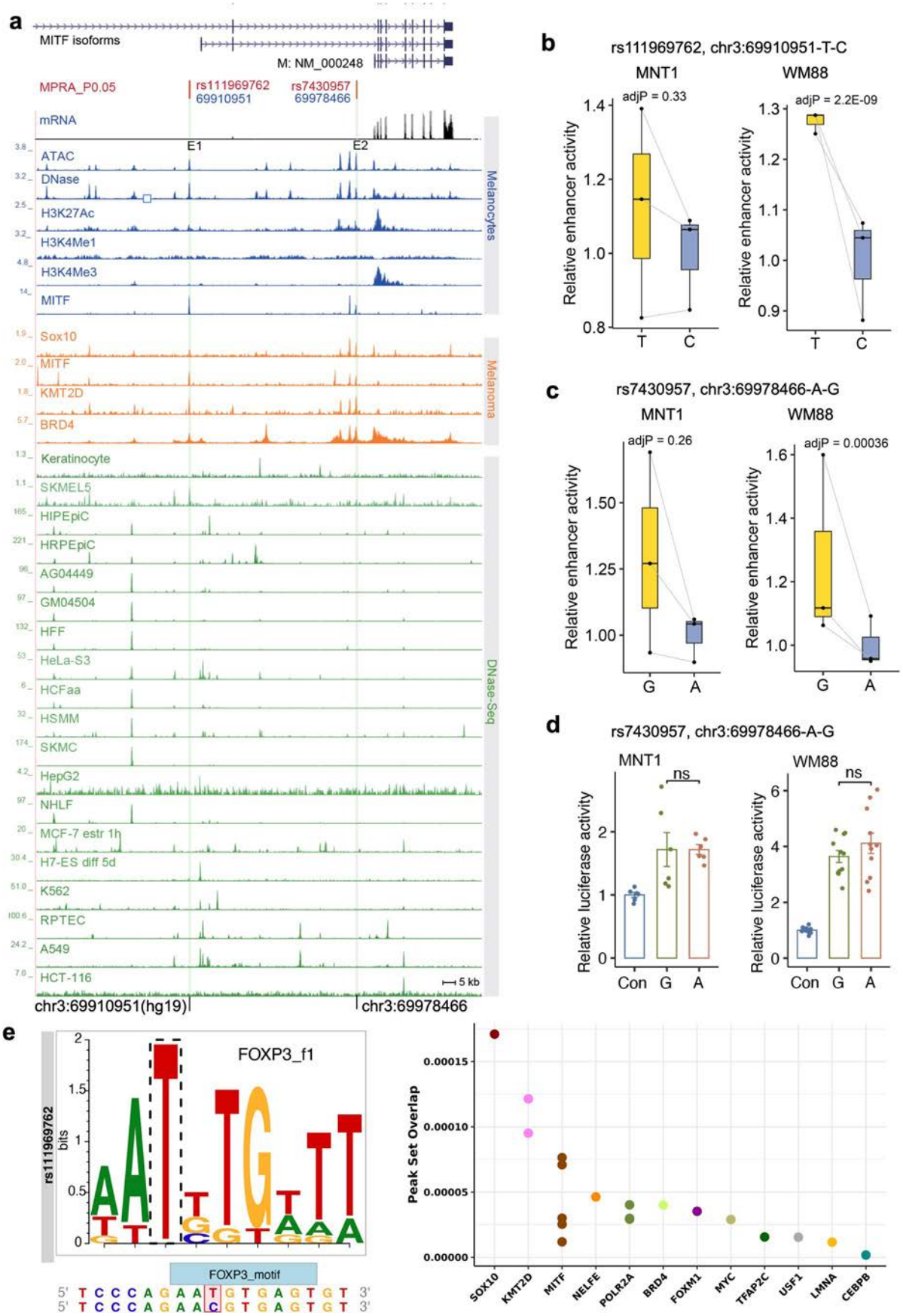

Extended Data Fig. 5 | See next page for caption.

https://doi.org/10.1038/s41588-023-01626-1

Extended Data Fig. 5 | Identification of functional variants near *MITF* related to skin pigmentation in the San. (**a**) A Plot showing functional Di-SNP rs111969762 is in a melanocyte-specific regulatory region. Blue tracks indicate DNase-Seq, ATAC-Seq, and ChIP-Seq from melanocytes; orange tracks indicate ChIP-Seq from melanoma (501-mel) cells; green tracks indicate DNase-Seq from ENCODE cell lines. E1-E2, enhancers. (**b**) MPRA showed that rs111969762 affects enhancer activity in WM88 cells (n = 3). (**c**) MPRA shows that rs7430957 impacts enhancer activity in WM88 cells (n = 3). (**d**) LRA shows that rs7430957 does not significantly alter the activity of the E2 enhancer near *MITF*. P values were estimated by two-tailed paired t-tests, MNT-1(n = 6), WM88 (n = 11). Data were presented as mean ± SEM. ns $p > 0.05$. (**e**) rs111969762 overlaps transcription factor binding sites. Left panel showed rs6497271 disrupts the binding motif of FOXP3. Right panel showed that rs111969762 overlaps ChIP-seq peaks from the Cistrome database[103]. MPRA p-values were estimated with a random effects model for mpralm and paired t-tests with multiple testing adjustments. For MPRA boxplots, central lines are median, with boxes extending from the 25th to the 75th percentiles. Whiskers further extend by ±1.5 times the interquartile range from the limits of each box.

https://doi.org/10.1038/s41588-023-01626-1

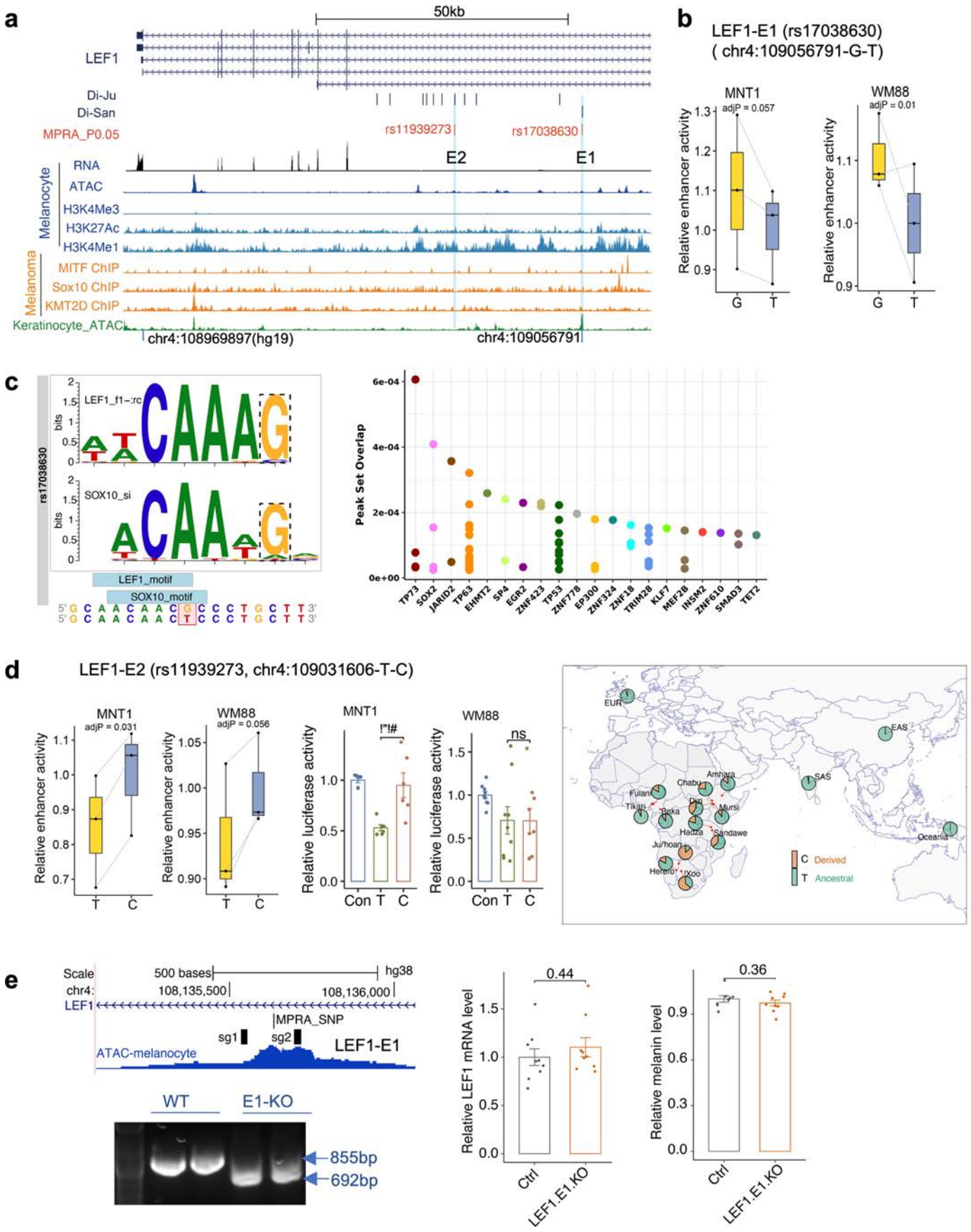

Extended Data Fig. 6 | See next page for caption.

https://doi.org/10.1038/s41588-023-01626-1

Extended Data Fig. 6 | Functional testing of Di-SNPs near *LEF1*. (**a**) MFVs and regulatory elements near *LEF1*. rs17038630 and rs11939273 are Di-SNPs from the San population. (**b**) Plot showing allelic skews at rs17038630 in MNT-1 and WM88 cells estimated by MPRA (n = 3). (**c**) rs17038630 overlaps SOX10 and LEF1 binding sites. Left panel shows that rs17038630 disrupts the binding motif of SOX10 and LEF1. Right panel shows that rs11939273 overlaps ChIP-seq peaks from the Cistrome database[103]. (**d**) MPRA and LRA results showing allelic skews at Di-SNP rs11939273 in MNT-1 and WM88 cells, the allele frequency data was from the 180 G[18] and 1000 G[31] dataset. MPRA (n = 3), LRA (MNT-1, n = 6; WM88, n = 9). LRA data are presented as mean ± SEM, tested with two-tailed paired t-tests. (**e**) CRISPR-KO of the enhancer E1 of *LEF1* does not affect LEF1 expression and melanin levels in MNT-1 cells. Left panel shows genotyping results of CRISPR-KO of the enhancer E1 of *LEF1*, three independent experiments. Middle panel shows the RT-qPCR results of CRISPR-KO of the enhancer E1 of *LEF1* (n = 9). Right panel shows the melanin levels of CRISPR-KO of the enhancer E1 of *LEF1* (n = 9). Two-tailed unpaired t-tests. For MPRA boxplots in b and d, central lines are median, with boxes extending from the 25th to the 75th percentiles. Whiskers further extend by ±1.5 times the interquartile range from the limits of each box. MPRA p-values were estimated with a random effects model for mpralm and paired t-tests with multiple testing adjustments.

https://doi.org/10.1038/s41588-023-01626-1

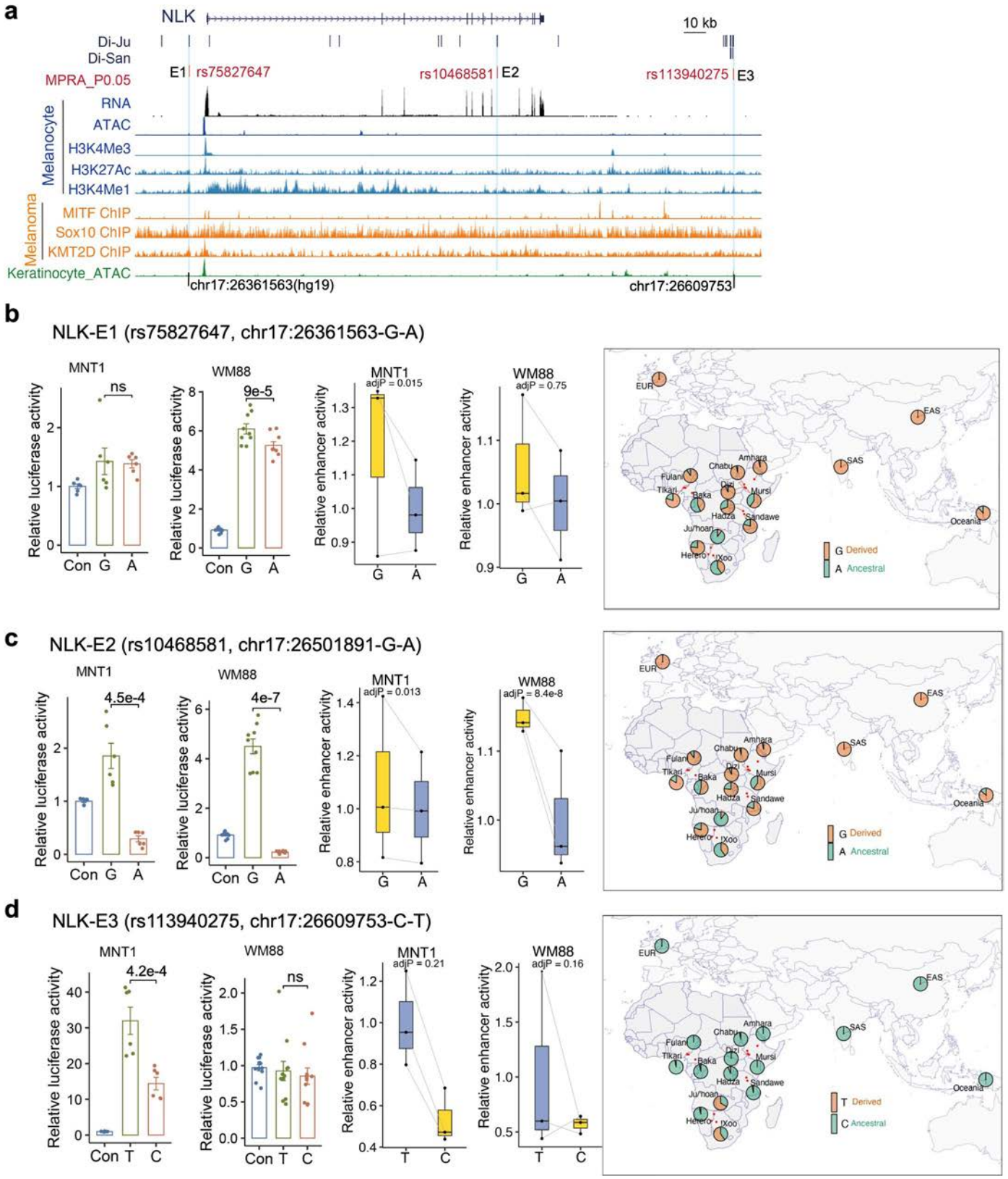

Extended Data Fig. 7 | MPRA and LRA identified three functional Di-SNPs near *NLK*. (**a**) MFVs and regulatory elements near *NLK*. rs75827647, rs10468581 and rs113940275 are Di-SNPs from the San population. (**b**) LRA and MPRA results showing allelic skews at rs75827647 in MNT-1 and WM88 cells. MPRA (n = 3), LRA (MNT-1, n = 6; WM88, n = 9). (**c**) LRA and MPRA results showing allelic skews at rs10468581 in MNT-1 and WM88 cells. MPRA (n = 3), LRA (MNT-1, n = 6; WM88, n = 9). (**d**) LRA and MPRA results showing allelic skews at rs113940275 in MNT-1 and WM88 cells. MPRA (n = 3), LRA (MNT-1, n = 6; WM88, n = 11). From b to d, the barplots are results of LRA, two-tailed paired t-tests without adjustments for multiple comparisons; data were presented as mean ± SEM. ns $p > 0.05$. The boxplots are results from MPRA, p-values were estimated with a random effects model for mpralm and paired t-tests with multiple testing adjustments. The right panels are allele frequency maps constructed using the 180G[18] and 1000 G[31] dataset. For boxplots, central lines are median, with boxes extending from the 25th to the 75th percentiles. Whiskers further extend by ±1.5 times the interquartile range from the limits of each box.

https://doi.org/10.1038/s41588-023-01626-1

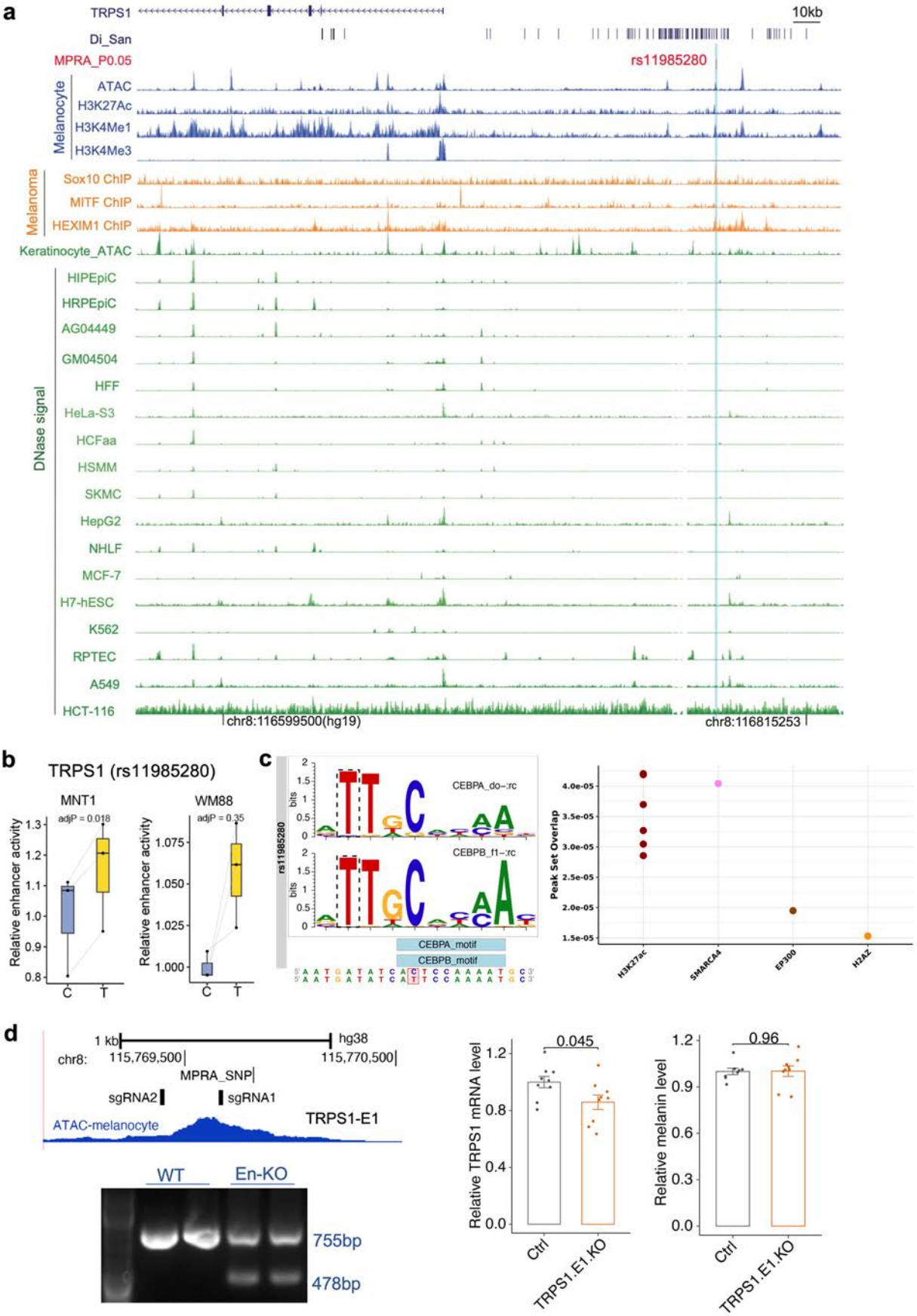

Extended Data Fig. 8 | See next page for caption.

https://doi.org/10.1038/s41588-023-01626-1

Extended Data Fig. 8 | Functional testing of Di-SNPs near *TRPS1*. (**a**) SNP rs11985280 overlaps a regulatory element of *TPRS1*. Blue tracks show ATAC-Seq, and ChIP-Seq data from melanocytes; orange tracks indicate ChIP-Seq data from melanoma (501-mel) cells, green tracks indicate ATAC-Seq and DNase-Seq data from ENCODE cell lines. (**b**) MPRA results showing allelic skews at rs11985280 in MNT-1 and WM88 cells (n = 3). p-values were estimated with a random effects model for mpralm and paired t-tests with multiple testing adjustments. For boxplots, central lines are median, with boxes extending from the 25th to the 75th percentiles. Whiskers further extend by ±1.5 times the interquartile range from the limits of each box. (**c**) rs11985280 disrupts the binding motif of CEBPA and CEBPB. Right panel shows that rs11985280 overlaps ChIP-seq peaks from the Cistrome database[103]. (**d**) CRISPR-KO of the enhancer E1 of *TRPS1* affects *TRPS1* expression but not melanin levels in MNT-1 cells. Left panel shows genotyping results of CRISPR-KO of the enhancer E1 of *TRPS1*, three independent experiments. Middle panel shows the RT-qPCR results of CRISPR-KO of the enhancer E1 of *TRPS1* (n = 9). Right panel shows the melanin levels of CRISPR-KO of the enhancer E1 of *TRPS1* in MNT-1 cells (n = 9). Two-tailed unpaired t-tests. Data are presented as mean ± SEM and p values are listed above the bars.

https://doi.org/10.1038/s41588-023-01626-1

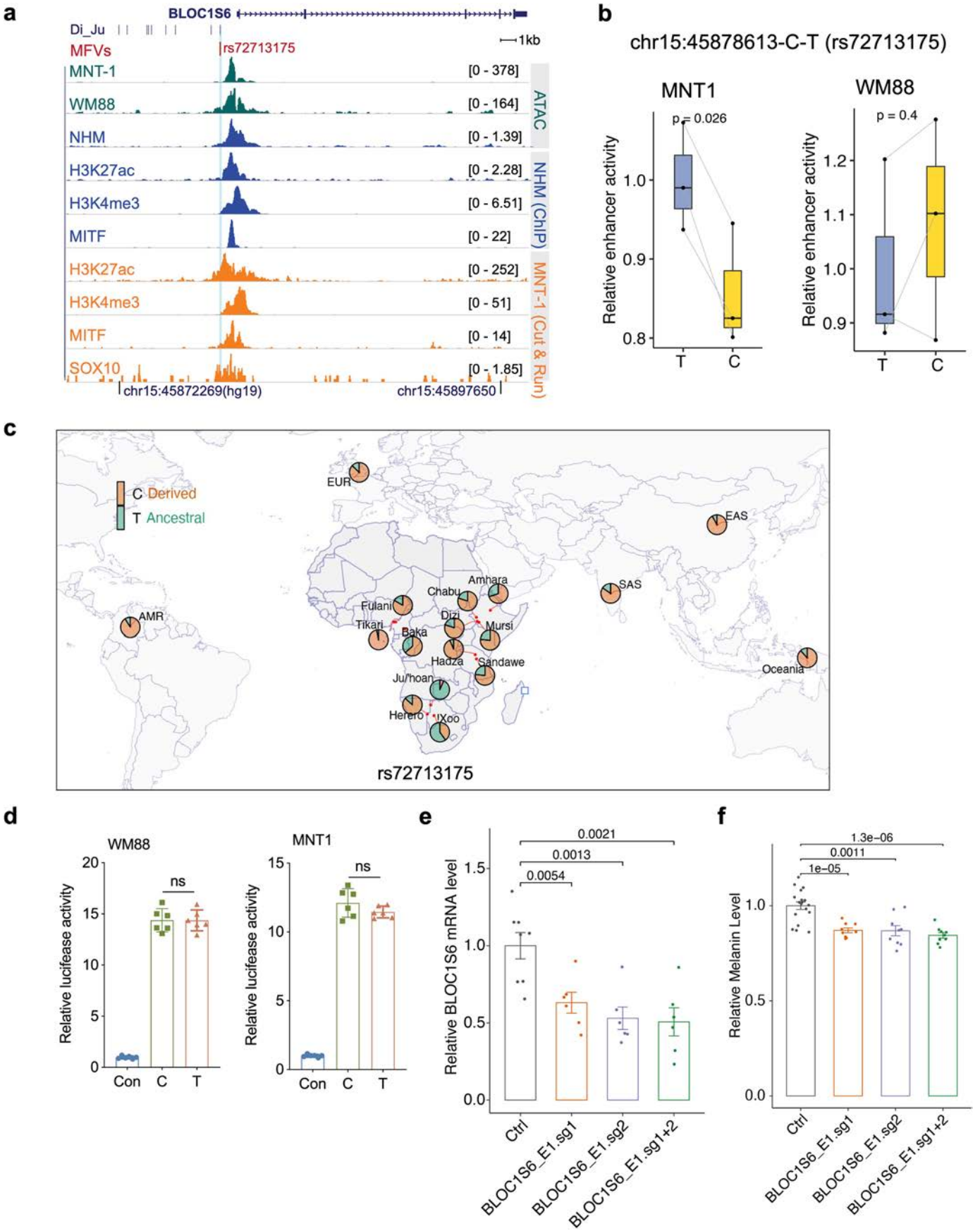

Extended Data Fig. 9 | See next page for caption.

https://doi.org/10.1038/s41588-023-01626-1

Extended Data Fig. 9 | Identification of functional regulatory variants near the *BLOC1S6* locus. (**a**). rs72713175 overlaps a regulatory region in melanocytes. Green tracks indicate ATAC-seq for MNT-1 and WM88 cells; blue tracks indicate ATAC-seq and ChIP-Seq from NHM; orange tracks indicate CUT&RUN from MNT-1 cells. (**b**) MPRA results showing allelic skews at rs11985280 in WM88 cells but not in MNT-1 cells (n = 3). P values were estimated with a random effects model for mpralm and paired t-tests without multiple testing adjustments. For boxplots, central lines are median, with boxes extending from the 25th to the 75th percentiles. Whiskers further extend by ±1.5 times the interquartile range from the limits of each box. (**c**) Allele frequencies at rs72713175 in global populations, data were from the 180 G[18] and 1000 G[31] datasets. (**d**) LRA results showing that rs72713175 did not affect enhancer activity in WM88 and MNT-1 cells. Two-tailed paired t-tests (n = 6). (**e**) CRISPRi of the enhancer containing rs72713175 significantly reduced the expression of *BLOC1S6* (control, n = 8; others, n = 6; Two-sided Dunnett's test with adjustments for multiple comparisons). (**f**) CRISPRi of the enhancer containing rs72713175 significantly reduced melanin levels in MNT-1 cells (control, n = 18; others, n = 9, Two-sided Dunnett's test with adjustments for multiple comparisons). Data are presented as mean ± SEM and p values are listed above the bars.

https://doi.org/10.1038/s41588-023-01626-1

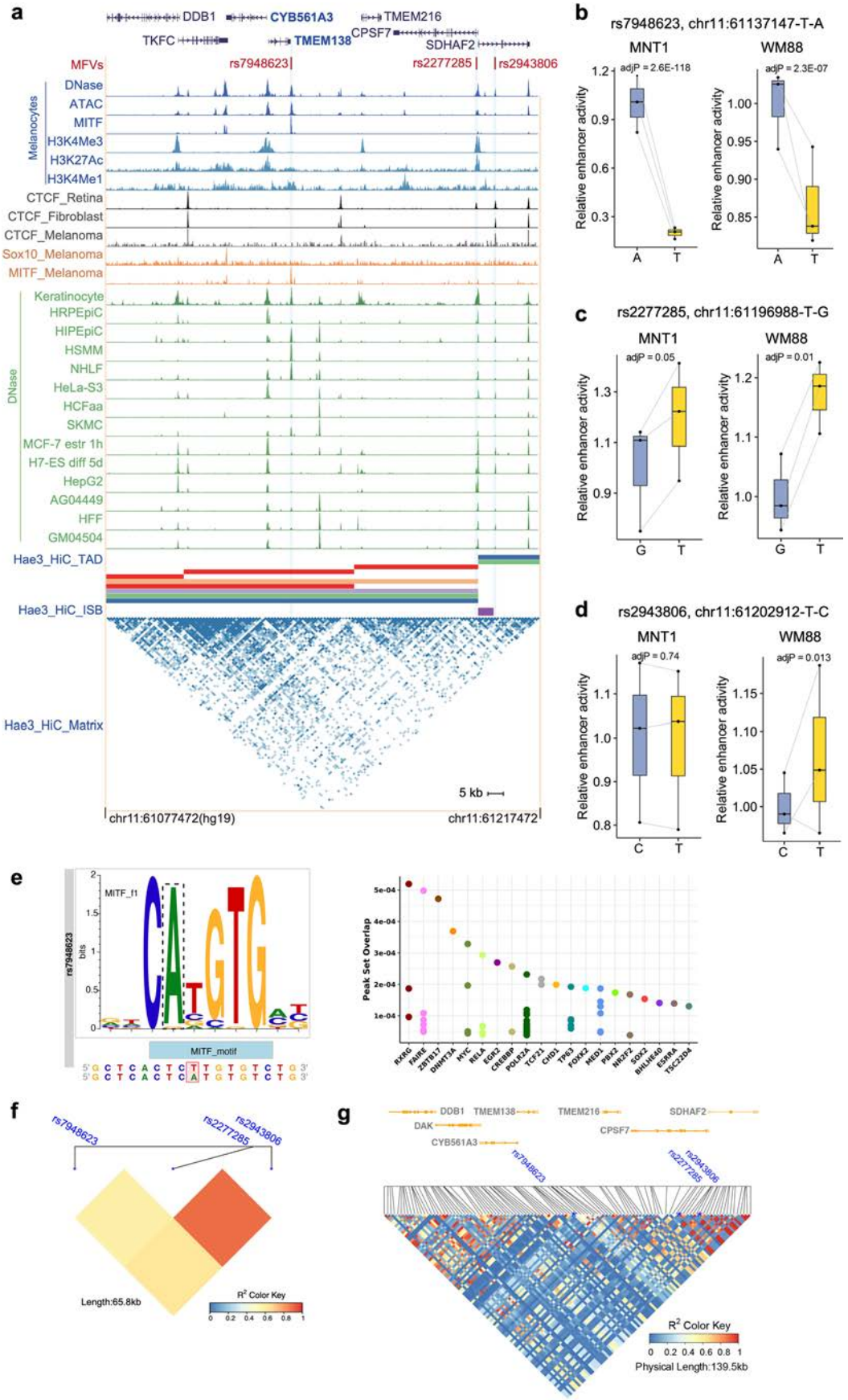

Extended Data Fig. 10 | See next page for caption.

https://doi.org/10.1038/s41588-023-01626-1

Extended Data Fig. 10 | Identification of functional regulatory variants near the *DDB1* locus. (**a**) Plots showing allelic skewed variants in regulatory elements near the *DDB1* locus. rs7948623 overlaps an open chromatin region in melanocytes and many other cell types. rs2277285 and rs2943806 are located within CTCF binding sites and TAD boundaries. Blue tracks indicate DNase-seq, ATAC-seq, and ChIP-Seq data from melanocytes; orange tracks indicate ChIP-Seq data from melanoma (501-mel) cells; gray tracks indicate CTCF ChIP-Seq data from three cell lines; and green tracks indicate DNase-Seq data from ENCODE[68]. (**b-d**) Allelic skews at rs7948623, rs2277285 and rs2943806 as estimated by MPRA (n = 3). P values were estimated with a random effects model for mpralm and paired t-tests without multiple testing adjustments. For boxplots, central lines are median, with boxes extending from the 25th to the 75th percentiles. Whiskers further extend by ±1.5 times the interquartile range from the limits of each box. (**e**) rs7948623 disrupts a MITF binding motif and overlaps ChIP-seq peaks from the Cistrome database[103]. (**f**, **g**) LD pattern between the MFVs at the *DDB1* locus. LD was calculated using the 180G[18] dataset.

nature portfolio

Corresponding author(s): Sarah Tishkoff

Last updated by author(s): Jul 13, 2023

Reporting Summary

Nature Portfolio wishes to improve the reproducibility of the work that we publish. This form provides structure for consistency and transparency in reporting. For further information on Nature Portfolio policies, see our Editorial Policies and the Editorial Policy Checklist.

Statistics

For all statistical analyses, confirm that the following items are present in the figure legend, table legend, main text, or Methods section.

n/a	Confirmed
☐	☒ The exact sample size (*n*) for each experimental group/condition, given as a discrete number and unit of measurement
☐	☒ A statement on whether measurements were taken from distinct samples or whether the same sample was measured repeatedly
☐	☒ The statistical test(s) used AND whether they are one- or two-sided *Only common tests should be described solely by name; describe more complex techniques in the Methods section.*
☐	☒ A description of all covariates tested
☐	☒ A description of any assumptions or corrections, such as tests of normality and adjustment for multiple comparisons
☐	☒ A full description of the statistical parameters including central tendency (e.g. means) or other basic estimates (e.g. regression coefficient) AND variation (e.g. standard deviation) or associated estimates of uncertainty (e.g. confidence intervals)
☐	☒ For null hypothesis testing, the test statistic (e.g. *F*, *t*, *r*) with confidence intervals, effect sizes, degrees of freedom and *P* value noted *Give P values as exact values whenever suitable.*
☒	☐ For Bayesian analysis, information on the choice of priors and Markov chain Monte Carlo settings
☒	☐ For hierarchical and complex designs, identification of the appropriate level for tests and full reporting of outcomes
☐	☒ Estimates of effect sizes (e.g. Cohen's *d*, Pearson's *r*), indicating how they were calculated

Our web collection on statistics for biologists contains articles on many of the points above.

Software and code

Policy information about availability of computer code

Data collection	We used GNU Wget v1.21.3 to download data from ENCODE. No other codes were used to collect data.
Data analysis	All softwares used in this study are public available, see details in https://docs.google.com/document/d/1ihhKTXonkmR_W2yTwvDpaRmDhsZt2ygU. The GWAS was conducted using a linear mixed model (EMMAX) implemented in EPACTS (Efficient and Parallelizable Association Container Toolbox, v3.3.0), and using kinship, sex, age, and top 10 PCs as covariates. Di analysis was performed by the method in https://doi.org/10.1073/pnas.0909918107. MPRA data was analyzed using FLASH v1.2.11, BWA 0.7.17, R package "mpra" version 1.18.0. HiC data were analyzed using fastp version 0.20.1, BWA 0.7.17, pairtools v1.01, cooltools v0.5.1, bedtools v2.29.2, onTADv1.4, FitHiChIP v10.0, cLoops v0.93, Mustache v1.0.1, plotgardener v1.2.10. CRISPR data was analyzed using CRISPResso v2.0.45, RNA-Seq data was analyzed using kallisto v0.46.2, DESeq2 v1.36.0, pathway enrichment was performed using GAGE v2.46.1 and pathview v1.36.1. SNP enrichment was performed using GREAT version 4.0.4. Transcription binding sites were predicted using motifbreakR

For manuscripts utilizing custom algorithms or software that are central to the research but not yet described in published literature, software must be made available to editors and reviewers. We strongly encourage code deposition in a community repository (e.g. GitHub). See the Nature Portfolio guidelines for submitting code & software for further information.

Data

Policy information about availability of data

All manuscripts must include a data availability statement. This statement should provide the following information, where applicable:

- Accession codes, unique identifiers, or web links for publicly available datasets
- A description of any restrictions on data availability
- For clinical datasets or third party data, please ensure that the statement adheres to our policy

RNA-Seq and epigenomic data is uploaded in GEO
Accession ID: GSE240717
Databank URL: https://www.ncbi.nlm.nih.gov/geo/query/acc.cgi?acc=GSE240717

The HiC data is uploaded in UCSC browser
Accession URL: https://genome.ucsc.edu/s/fengyq/Tishkoff_Lab%2Dhg38%2DMPRA%2DHiC_Pigmentation

Genotype data for GWAS is in dbGaP: phs001396.v1.p1. Genotype data for Di analysis is under processing dbGaP.

SNP frequency data is in the supplementary tables.

Public data are from https://www.proteinatlas.org/, https://www.encodeproject.org/, https://www.gtexportal.org/home/, https://www.ebi.ac.uk/gwas/, https://genetics.opentargets.org/. KEGG database, GREAT website, GO database, dbSNP database.

Human research participants

Policy information about studies involving human research participants and Sex and Gender in Research.

Reporting on sex and gender	For individuals used in the GWAS, sex are evenly represented (768 males and 825 females) and self reported ages ranged from 18 to 103. Mean age was used for individuals without ages. See details in Crawford et al (https://www.science.org/doi/10.1126/science.aan8433) and dbGaP:phs001396.v1.p1.
Population characteristics	For individuals used in the GWAS, see detailed population characteristics in Crawford et al (https://www.science.org/doi/10.1126/science.aan8433) and dbGaP: phs001396.v1.p1.
Recruitment	Recruitment was voluntary for all participants.
Ethics oversight	Before sample collection, we obtained permits from local institutions in Africa. An appropriate IRB approval was also obtained from the University of Pennsylvania. All individuals involved in this study have approved written informed consents.

Note that full information on the approval of the study protocol must also be provided in the manuscript.

Field-specific reporting

Please select the one below that is the best fit for your research. If you are not sure, read the appropriate sections before making your selection.

☒ Life sciences ☐ Behavioural & social sciences ☐ Ecological, evolutionary & environmental sciences

For a reference copy of the document with all sections, see nature.com/documents/nr-reporting-summary-flat.pdf

Life sciences study design

All studies must disclose on these points even when the disclosure is negative.

Sample size	No statistical method was used to predetermine the sample size as we used the samples from published datasets. For experimental validations, we performed > 3 biological replicates for MPRA, luciferase reporter assays, and CRISPR-based experiments to do the statistical test of significance.
Data exclusions	No other data were excluded.
Replication	All cell-based experiments were repeated independently at least 3 times. All attempts at replication were successful.
Randomization	We randomly selected controls for MPRA, see methods; For confocal images and related quantification of MNT-1 cells, the cells were randomly selected.
Blinding	No blinding were used for this study.

Reporting for specific materials, systems and methods

We require information from authors about some types of materials, experimental systems and methods used in many studies. Here, indicate whether each material, system or method listed is relevant to your study. If you are not sure if a list item applies to your research, read the appropriate section before selecting a response.

Materials & experimental systems

n/a	Involved in the study
☐	☒ Antibodies
☐	☒ Eukaryotic cell lines
☒	☐ Palaeontology and archaeology
☒	☐ Animals and other organisms
☒	☐ Clinical data
☒	☐ Dual use research of concern

Methods

n/a	Involved in the study
☒	☐ ChIP-seq
☒	☐ Flow cytometry
☒	☐ MRI-based neuroimaging

Antibodies

Antibodies used

Anti-Histone H3 (acetyl K27); Rabbit Abcam Cat#ab4729; RRID: AB_2118291, 1:50 dilution.
Anti-H3K4me3; Rabbit epicypher Cat#13-0041; RRID: NA, 1:50 dilution.
IgG; Rabbit epicypher Cat#13-0042; RRID: NA, 1:50 dilution.
Anti-GFP; Rabbit Abcam Cat#ab290; RRID: AB_303395, 1:200 dilution.
Anti-GAPDH; Mouse Santa Cruz Cat#sc-47724; RRID: AB_627678, 1:1000 dilution.
Anti-TYRP1; Mouse BioLegend Cat#SIG-38150; RRID: AB_10175227, 1:200 dilution.
Anti-LAMP2; Mouse DSHB Cat# H4A3; RRID: AB_626858, 1:200 dilution.
Anti-HA; Rat Roche Cat# ROAHAHA, RRID: AB_2687407, 1:1000 dilution.
Anti-SOX10; Rabbit CST Cat#89356; RRID: AB_2792980, 1:50 dilution.
Anti-MITF; Rabbit CST Cat#12590; RRID: AB_2616024, 1:50 dilution.

Validation

Validation studies were performed by the commercial vendor (use the catalog and lot number listed above to access this data on the websites of the vendors)

Eukaryotic cell lines

Policy information about cell lines and Sex and Gender in Research

Cell line source(s)

MNT-1 cells (ATCC, #CRL- 3450), a gift from Dr. Michael S. Marks at Children's Hospital of Philadelphia Research Institute.
WM88 cells (rockland, WM88-01-0001), a melanocytic patient-derived melanoma tumor cell line, a gift from Dr. Ashani Weeraratna at Wistar Institute
HeLa cells (CCL-2, ATCC), Lenti-X 293T cells (Takara, # 632180)

Authentication

MNT-1 and WM88 were confirmed by our collaborators; HeLa cells and Lenti-X 293T cells were guaranteed by vendors.

Mycoplasma contamination

MNT-1, WM88, HeLa and Lenti-X 293T cells were tested negative for Mycoplasma contamination

Commonly misidentified lines
(See ICLAC register)

None